The signal-to-background ratio, in particular, which is $\sim\frac{1}{2}$ at 2.8 and 3.8 GeV/c, becomes $\sim\frac{1}{4}$ at 5 GeV/c.

[17]J. D. Boright *et al.*, Phys. Lett. 33B, 615 (1970).

[18]R. C. Chase *et al.*, Phys. Lett. 30B, 659 (1969).

[19]We mention that from a bubble-chamber experiment [see Ref. 10 and also A. Rougé *et al.*, Nucl. Phys. B44, 365 (1972); L. Moscoso *et al.*, paper No. 90 presented to the Amsterdam International Conference on Elementary Particles, 1971 (unpublished)] at 3.95 GeV/c the cross sections for $K^-p \to \pi^0\Lambda$, $\eta\Lambda$, $X^0\Lambda$ integrated over the backward peak are quoted as 9.07 ± 1.27, 2.1 ± 1.5, and 0.0 ± 0.1 μb, respectively.

[20]V. Barger *et al.* [Nucl. Phys. 49B, 206 (1972)] point to a value between 0.25 and 0.4, analyzing processes supposedly dominated by N_α exchange, in agreement with a similar analysis of B. Kayser and F. Hayot [Phys. Rev. D 6, 2423 (1972)]. Analyses of processes corresponding to the more complicated hyperon exchange point to values fluctuating around 0.5 [B. Kayser and F. Hayot, Phys. Rev. D 6, 2423 (1972); R. L. Eisner *et al.*, *ibid.* 7, 1 (1973); G. W. Brandenburg *et al.*, Phys. Rev. Lett. 30, 145 (1973)].

[21]G. Ebel *et al.*, in *Proceedings of the Fifth International Conference on Elementary Particles, Lund, 1969*, edited by G. von Dardel (Berlingska, Lund, Sweden, 1970), p. 411.

[22]H. Ebenhoh *et al.*, Z. Phys. 241, 473 (1971).

[23]See L. F. Li and H. Pagels, Phys. Rev. D 5, 1509 (1972), for a theoretical prediction [$F/(F+D) = 0.3$] concerning this quantity.

[24]M. Aguilar-Benitez *et al.*, Phys. Rev. Lett. 25, 1635 (1970); R. L. Eisner, in *Experimental Meson Spectroscopy—1972*, edited by Kwan-Wu Lai and A. H. Rosenfeld (Ref. 9), p. 107.

[25]H. Brody, University of Pennsylvania report 1972 (unpublished), as quoted by R. Diebold, Rapporteur's talk, in *Proceedings of the XVI International Conference on High Energy Physics, Chicago-Batavia, Ill., 1972*, edited by J. D. Jackson and A. Roberts (NAL, Batavia, Ill., 1973), Vol. 3, p. 1.

PHYSICAL REVIEW D VOLUME 8, NUMBER 9 1 NOVEMBER 1973

Role of $\gamma + \gamma \to e^+ + e^- + e^+ + e^-$ in Photoproduction, Colliding Beams, and Cosmic Photon Absorption*

R. W. Brown,† W. F. Hunt,† and K. O. Mikaelian†
Case Western Reserve University, Cleveland, Ohio 44106

I. J. Muzinich*
Brookhaven National Laboratory, Upton, New York 11973

(Received 9 July 1973)

We consider the photon-photon channel, $\gamma + \gamma \to e^+ + e^- + e^+ + e^-$, with respect to the possible relevant experimental roles it plays in (i) the photoproduction process $\gamma + Z \to Z + e^+ + e^- + e^+ + e^-$, (ii) the colliding beam process $e^\pm + e^- \to e^\pm + e^- + e^+ + e^- + e^+ + e^-$, and (iii) the absorption of high-energy cosmic photons. Discussion of the first role includes calculation of rates at different energies, error estimates, and effects of screening and threshold cuts. In the second role, emphasis is placed on scale changes due to energy and angle kinematic cuts. Competition with the single-pair absorption process (i.e., $\gamma + \gamma \to e^+ + e^-$) at the higher cosmic γ-ray energies $\approx 10^{20}$ eV is discussed in the consideration of the third role.

I. INTRODUCTION

In the past few years, we have seen the fascinating emergence of the importance and even dominance of higher-order quantum-electrodynamic (QED) processes at high energies. It is probably accurate to state that these developments began with the study of all elastic two-body amplitudes by Cheng and Wu.[1] In electron Compton scattering, for example, they showed that for large center-of-momentum (c.m.) energy $\sqrt{s}$ the second- and fourth-order amplitudes approach a constant while the sixth-order amplitude increases proportionally with s (ln$s$ factors are disregarded in these statements). Further theoretical research[2,3] showed that two-photon intermediate states were more important at higher energies than the single-photon annihilation process in hadron production through electron-positron collisions. In fact, detailed calculations by Brodsky, Kinoshita, and Terazawa[3] demonstrated that pion production via the two-photon mechanism was more probable at beam energies as low as 2 GeV. This mechanism has already been taken into account as a background in single-photon data.[4]

The reason for the importance of higher-order processes can be presented rather simply in terms of the "scale" of the cross sections involved. The inverse-mass-squared dimension necessary for a cross-section expression is provided by s^{-1} in many lowest-order calculations. [See Eq. (1.2) below for an example of this.] However, the scale can be set by some particle's mass m in some of the higher-order "corrections" to these calcula-

tions, with the end result that corrections dominate at large enough s. A specific example is real photon-photon collisions, which are central to our work here and will be discussed in detail. It is important to note that once the cross sections are found to be constant $\sim m^{-2}$ (within logarithms) in some order, we do not continue to find higher corrections with higher powers of s/m^2. (This would certainly overshoot unitarity bounds quickly.) Rather, we find only additional powers of logarithms which cannot overcome the concomitant powers of α/π for any practical energy regime.

The aforementioned photon-photon example is the higher-order (fourth-order) two-pair creation

(i) $\gamma+\gamma\to e^+ + e^- + e^+ + e^-$,

whose asymptotic cross section is constant[5,6]:

$$\sigma_{\rm i}(s)\cong \frac{\alpha^4}{36\pi m^2}[\,175\zeta(3)-38]\cong 6.45\ \mu{\rm b}, \qquad s/m^2\to\infty . \quad (1.1)$$

Here m is the electron mass and $\zeta(3)\cong 1.202$ is the zeta function with argument 3. The lower-order single-pair creation

(ii) $\gamma+\gamma\to e^+ + e^-$

has an asymptotically decreasing cross section[7]:

$$\sigma_{\rm ii}(s)\cong \frac{4\pi\alpha^2}{s}[\,\ln(s/m^2)-1], \quad s/m^2\to\infty . \quad (1.2)$$

We see that Reaction (i) dominates over (ii) when $s\gtrsim 1\ {\rm GeV}^2$, a circumstance which motivated most of the work reported here.[8,9] Part of this work reports on the details of the earlier work.[8] We address ourselves to the possibility that study of Reaction (i) will lead directly or indirectly to relevant experimental statements.

Since we do not have photon "targets" readily available to use in the laboratory, we are led to consider (a) the possibility of using virtual photons (whose source is electron or nuclear currents) for initiating Reaction (i), or (b) the background radiation permeating the universe as targets for the high-energy γ-ray component in cosmic rays. The first consideration is introduced in more detail below, after which the introduction to the second is also expanded.

The first possibility suggests looking at

(iii) $\gamma+Z\to Z+e^+ + e^- + e^+ + e^-$

as a generalized Primakoff-type reaction where the Coulomb interaction of the nuclear target (Z) provides us with a spacelike virtual photon. The intermediate-state reaction then resembles Reaction (i), and a leading-logarithm expression for Reaction (iii) is[8,10]

$$\sigma_{\rm iii}(\omega)\cong Z^2\,\frac{\alpha}{\pi}\sigma_{\rm i}(\infty)\ln^2(\omega/m), \quad \omega/m\to\infty \quad (1.3)$$

where $\sigma_{\rm i}(\infty)$ is given by Eq. (1.1) and ω is the photon energy in the rest frame of the target. As we will see, this is not a very good estimate of the total cross section for ω values of practical interest since the nonleading-logarithm corrections are nonvanishing and hence important. [The corrections to the brackets in (1.1) and (1.2) vanish like $(m^2/s)\times$powers of $\ln(s/m^2)$ and so are not vital there; a similar remark applies to Eq. (1.4) below.]

For comparison with Reaction (iii), we note that the Bethe-Heitler reaction

(iv) $\gamma+Z\to Z+e^+ + e^-$

has the leading behavior[11]

$$\sigma_{\rm iv}(\omega)\cong Z^2\,\frac{\alpha^3}{27m^2}[\,84\ln(2\omega/m)-218], \qquad \omega/m\to\infty . \quad (1.4)$$

This does *not* have its scale set by s^{-1}, and thus is much larger than (1.3) for any energy regime of interest. The philosophy is changed then insofar as our interest in Reaction (iii) vis-à-vis Reaction (iv) is concerned, since we cannot expect (iii) to be dominant anywhere. Rather, we rely on the possibility that a four-electron final state may furnish a sufficiently unique signature under the appropriate experimental conditions. Since the rates we find for (iii) are fairly large, the hope is that this reaction could be seen in the near future.

Continuing the search for virtual photon "beams," we can also examine the dominant contribution to

(v) $e^\pm + e^- \to e^\pm + e^- + e^+ + e^- + e^+ + e^-$

as another indirect test of Reaction (i). The electron currents are the virtual photon sources here, and an asymptotic leading-logarithm expression has been given by Serbo and by Lipatov and Frolov[10]:

$$\sigma_{\rm v}(s)\cong \frac{1}{6}\,\frac{\alpha^2}{\pi^2}\sigma_{\rm i}(\infty)\ln^4(s/m^2), \quad s/m^2\to\infty . \quad (1.5)$$

This is a rough estimate.[12] Due to scale changes in the $\gamma\gamma\to 4e$ kernel, vanishing phase-space factors, and electron statistics, we expect that the $O(\ln^3 s)$ corrections are large and negative. [Notice the sign on the correction in Eq. (1.4).] A similar remark applies to the $O(\ln\omega)$ correction in Eq. (1.3).

We have the same point to make about Reaction (v) in comparison with the lower-order process

(vi) $e^\pm + e^- \to e^\pm + e^- + e^+ + e^-$

that was made in comparing (iii) with (iv). As

Landau and Lifshitz estimated long ago,[13]

$$\sigma_{\rm vi}(s)\cong\frac{28}{27}\frac{\alpha^4}{\pi m^2}\ln^3(s/m^2),\quad s/m^2\to\infty,\qquad(1.6)$$

which also has important corrections.[14] Only at absurdly large energies (where perturbation theory is suspect anyway) does (v) dominate over (vi).

We have less interest in (v) than in (iii). This is because the major part of the cross section derives from small angles and the necessary minimum angle cut away from the incoming electron beam will change the m^{-2} scale. This reduces the rates tremendously and lessens its impact on experiment. We discuss the change in scale later in this paper.

Finally, with respect to the consideration (b) mentioned earlier in this introduction, we are interested in the attenuation of high-energy γ rays traversing the background radiation in the universe.[15] As higher and higher energies become relevant to cosmic-ray research, we expect Reaction (i) to dominate according to the previous discussion. The region of overlap and the significance of such absorption is another of our goals.

The organization of our discussion and work is as follows: We present in Sec. II the basic ingredients in calculating the dominant contributions to the absorptive part of the $\gamma\gamma$ forward scattering amplitude for a given order in α. This includes off-mass-shell effects (in particular, scale changes) for virtual photons. Section III is directed toward a discussion of the viability of observing Reaction (iii) experimentally. Results more accurate than Eq. (1.3) are presented, as well as discussions about background and theoretical uncertainties. In Sec. IV, we consider the reductions in the cross section for (v) [and (vi) for comparison] if energy and angle cuts are made. The absorptions by Reactions (i) and (ii) are compared in Sec. V insofar as cosmic rays are concerned. A brief summary of all results comprises Sec. VI. There is an appendix which contains some Feynman-graph asymptotics.

II. OFF-MASS-SHELL CROSS SECTIONS FOR $\gamma\gamma\to e^+e^-e^+e^-$ AND $\gamma\gamma\to e^+e^-$

We describe here an exact (albeit numerical) calculation of the dominant high-energy contribution to the total cross section in Reaction (i). Reaction (ii), which is rather simple, is also treated in a parallel fashion, providing a comparison which will prove useful later. Having the energy and virtual-photon mass dependence of these cross sections at our disposal illustrates the scale changes of interest and also is necessary for later developments discussed in the next sections.

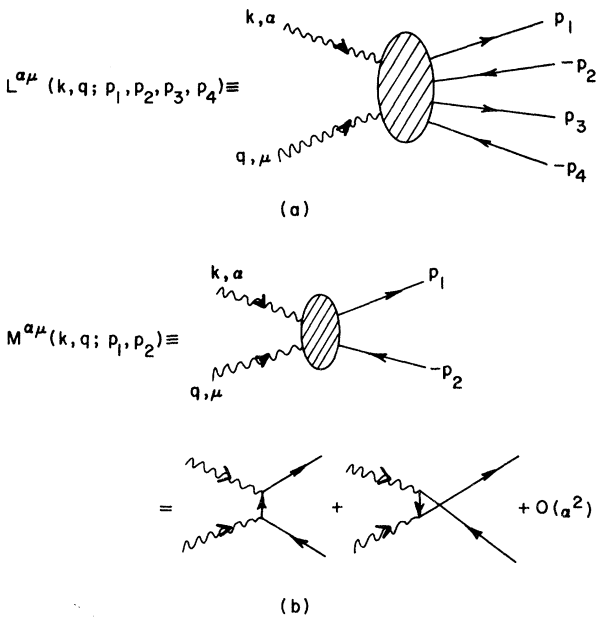

FIG. 1. The general Feynman amplitudes for (a) Reaction (i); (b) Reaction (ii).

The momentum and photon helicity assignments for the two processes are given in Fig. 1, where the general Feynman amplitudes are shown. For Reaction (i), the amplitude $L^{\alpha\mu}$ of Fig. 1(a) is represented by 40 Feynman diagrams in lowest (fourth) order. However, here we are interested only in the dominant contribution to the total cross section at high energy, $s'\gg|k^2|,|q^2|,m^2$, where

$$s'\equiv(k+q)^2=(p_1+p_2+p_3+p_4)^2$$

$$=\text{square of the c.m. energy},$$

$$p_i{}^2=m^2,$$

and

$$k^2\leq 0,\quad q^2\leq 0.$$

The calculation of this contribution involves much less work than might first be imagined; it is discussed most clearly in terms of absorptive parts of the forward elastic $\gamma\gamma$ amplitude which are related, of course, by the optical theorem to the cross sections of interest.

As a result of the discussion relegated to the Appendix, we find that the dominant absorptive parts are represented by 16 cut graphs summarized by Fig. 2(a).[16] That is, the contribution of the four-electron intermediate state, call it $A_{\beta\nu\alpha\mu}(k,q)$, is

$$A_{\beta\nu\alpha\mu}(k,q)=A^{\rm dom}_{\beta\nu\alpha\mu}(k,q)\times[1+(1/s')\times(\text{powers of }\ln s')]\qquad(2.1)$$

according to the arguments in the Appendix. (We discuss briefly the nondominant contribution at the end of this section.) Here $A^{\rm dom} \sim s'$ and leads to a constant cross section. Exploiting the factorized form by the identity

$$\delta^4\Big(\sum p_i - k - q\Big) = \int d^4r\, \delta^4(p_1+p_2-k-r) \times \delta^4(p_3+p_4+r-q), \quad (2.2)$$

we have

$$A^{\rm dom}_{\beta\nu\alpha\mu}(k,q) = \frac{1}{(2\pi)^8}\int \frac{d^4r}{r^4} T^{(1)}{}_{\beta\sigma\alpha\lambda}(k,r) \times T^{(2)\sigma}{}_{\nu}{}^{\lambda}{}_{\mu}(-r,q), \quad (2.3)$$

with ($p_{i0} \equiv E_i$)

$$T^{(1)}{}_{\beta\sigma\alpha\lambda}(k,r) \equiv \sum_{\rm spins}\int \frac{m}{E_1}d^3p_1\,\frac{m}{E_2}\,d^3p_2\,\delta^4(p_1+p_2-k-r) \times M^*_{\beta\sigma}(k,r;p_1,p_2)M_{\alpha\lambda}(k,r;p_1,p_2). \quad (2.4)$$

The function $T^{(2)}$ is obtained by the replacements $p_1 \to p_3$, $p_2 \to p_4$, $k \to -r$, and $r \to q$; thus, if the p_i integration regions are identical, the $T^{(i)}$ are the same functions. In lowest order, the $\gamma\gamma \to e^+e^-$ amplitudes look like [see Fig. 1(b)]

$$M_{\alpha\lambda}(k,r;p_1,p_2) = -ie^2\bar{u}(p_1)\left(\gamma_\alpha \frac{1}{\not p_1 - \not k - m}\gamma_\lambda + \gamma_\lambda \frac{1}{\not p_1 - \not r - m}\gamma_\alpha\right)v(p_2). \quad (2.5)$$

The absorptive part (2.3) is the basis for all of our four-electron calculations. Also, the absorptive part of the two-electron intermediate state is

$$B_{\beta\nu\alpha\mu}(k,q) = \frac{1}{(2\pi)^2}T^{(1)}{}_{\beta\nu\alpha\mu}(k,q), \quad (2.6)$$

which will be the basis for the parallel $\gamma\gamma \to e^+e^-$ discussion. This amplitude is also illustrated in Fig. 2.

We are concerned in this section with "generalized" cross sections for Reaction (i),

$$\tilde{\sigma}_{\rm i}(s',k^2,q^2) = \frac{1}{8s'}A_{\beta\nu}{}^{\beta\nu}(k,q), \quad (2.7)$$

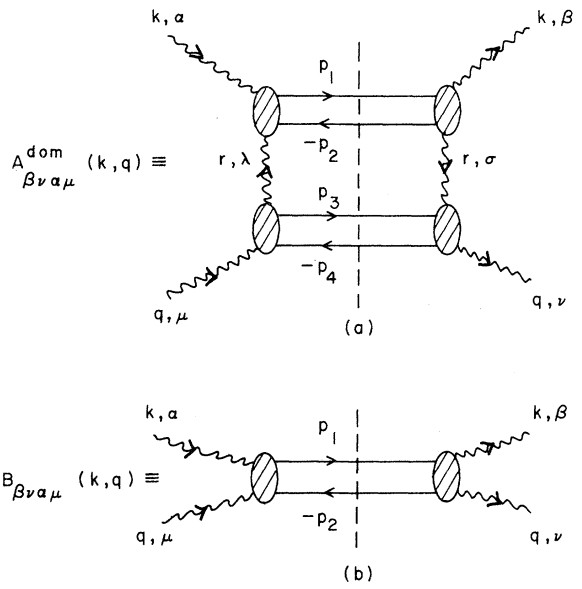

FIG. 2. (a) The dominant absorptive part at high energy for the forward $\gamma\gamma$ amplitude in order α^4. (b) The α^2 (lowest-order) absorptive part for the forward $\gamma\gamma$ amplitude. The blobs in both (a) and (b) correspond to the order-α terms explicitly shown in Fig. 1(b).

and for Reaction (ii),

$$\tilde{\sigma}_{\rm ii}(s',k^2,q^2) = \frac{1}{8s'}B_{\beta\nu}{}^{\beta\nu}(k,q). \quad (2.8)$$

These forms were chosen so as to display the change of scale for $k^2, q^2 < 0$ and such that in the limit $k^2 = q^2 = 0$ we obtain the corresponding physical cross sections for collinear unpolarized photon beams. Accordingly, we included a relative-velocity factor ($\frac{1}{2}$), a photon spin-average factor ($\frac{1}{4}$), and the photon wave-function normalization factors

$$\left(\frac{1}{2k^0}\frac{1}{2q^0} \equiv \frac{1}{2\omega_k}\frac{1}{2\omega_q}\right)$$

evaluated at $k^2 = q^2 = 0$. For real collinear photon beams, $s' = 4\omega_k\omega_q$. In Eq. (2.7), the electron statistics factor $1/2!\,2!$ is understood to be included in the definition of $A_{\beta\nu\alpha\mu}$.[16]

In terms of kinematic singularity- and zero-free invariant amplitudes,[17]

$$T^{(1)}{}_{\beta\sigma}{}^{\beta}{}_{\lambda}(k,r) = (g_{\sigma\lambda}r^2 - r_\sigma r_\lambda)t_1^{(1)}(k^2,r^2,s_1) + [r^2k_\sigma k_\lambda - k\cdot r(k_\sigma r_\lambda + r_\sigma k_\lambda) + (k\cdot r)^2 g_{\sigma\lambda}]\,t_2^{(1)}(k^2,r^2,s_1) \quad (2.9)$$

and

$$T^{(2)\sigma}{}_{\nu}{}^{\lambda\nu}(-r,q) = (g^{\sigma\lambda}r^2 - r^\sigma r^\lambda)t_1^{(2)}(r^2,q^2,s_2) + [r^2q^\sigma q^\lambda - r\cdot q(r^\sigma q^\lambda + q^\sigma r^\lambda) + (r\cdot q)^2 g^{\sigma\lambda}]\,t_2^{(2)}(r^2,q^2,s_2), \quad (2.10)$$

where $s_1 \equiv (k+r)^2$ and $s_2 \equiv (-r+q)^2$. Thus

$$A^{\rm dom}_{\beta\nu}(k,q)=\frac{1}{(2\pi)^8}\int\frac{d^4r}{r^4}\{3r^4t_1^{(1)}t_1^{(2)}+r^2[r^2q^2+2(r\cdot q)^2]t_1^{(1)}t_2^{(2)}+r^2[r^2k^2+2(k\cdot r)^2]t_2^{(1)}t_1^{(2)}$$
$$+[r^4(k\cdot q)^2-2r^2r\cdot qk\cdot rk\cdot q+r^2k^2(r\cdot q)^2+r^2q^2(k\cdot r)^2+2(k\cdot r)^2(r\cdot q)^2]t_2^{(1)}t_2^{(2)}\}. \tag{2.11}$$

We note in passing that the invariant amplitude $t_2^{(1)}$ is to be found in actual computation by the projection

$$t_2^{(1)}(k^2,r^2,s_1)=\frac{1}{2}\frac{1}{[(k\cdot r)^2-k^2r^2]^2}\{[(k\cdot r)^2-k^2r^2]T^{(1)}{}_{\beta\sigma}{}^{\beta\sigma}(k,r)+3r^2k^\sigma k^\lambda T^{(1)}{}_{\beta\sigma}{}^{\beta}{}_{\lambda}(k,r)\}, \tag{2.12}$$

after which we can determine $t_1^{(1)}$ by

$$t_1^{(1)}(k^2,r^2,s_1)=\frac{1}{3}\frac{1}{r^2}\{T^{(1)}{}_{\beta\sigma}{}^{\beta\sigma}(k,r)-[2(k\cdot r)^2+k^2r^2]t_2^{(1)}(k^2,r^2,s_1)\}. \tag{2.13}$$

By Bose symmetry, the $t_i^{(2)}$ are found by the same equation upon the substitutions $t_i^{(1)}\to t_i^{(2)}$, $T^{(1)}\to T^{(2)}$, and $k\to q$, $r\to -r$ [since Eqs. (2.12) and (2.13) involve only scalar quantities, this means $k^2\to q^2$, $r^2\to r^2$, $k\cdot r\to -r\cdot q$ $(s_1\to s_2)$].

Our procedure is to do analytically the p_i integrations [see Eq. (2.4)] for fixed r. That is, $T^{(1)}$ and $T^{(2)}$ enter into Eqs. (2.12) and (2.13) in Lorentz scalar form only. We can therefore integrate these forms in the $\vec{k}+\vec{r}=0$ and $-\vec{r}+\vec{q}=0$ c.m. frames, respectively, where the integration limits are trivial. So, after lengthy trace calculations and some simple polar-angle integrations, the $T^{(1)}$ contractions are

$$T^{(1)}{}_{\beta\sigma}{}^{\beta\sigma}(k,r)=e^4\pi\left(\frac{s_1-4m^2}{s_1}\right)^{1/2}\{-8+4(r^2+k^2-s_1-2m^2)I_1-4(2m^2+k^2)(2m^2+r^2)I_2$$
$$+4[(k^2+r^2)(s_1-m^2)+m^2(s_1-4m^2)]I_3\} \tag{2.14}$$

and

$$k^\sigma k^\lambda T^{(1)}{}_{\beta\sigma}{}^{\beta}{}_{\lambda}(k,r)=e^4\pi\left(\frac{s_1-4m^2}{s_1}\right)^{1/2}\{-4s_1+4m^2(r^2-k^2-s_1)I_1-2k^2s_1(2m^2+k^2)I_2$$
$$+2k^2[s_1(k^2+r^2)+2m^2(k^2-r^2)]I_3\}. \tag{2.15}$$

The I_i entering into the above are

$$I_1=\frac{1}{2|\vec{k}||\vec{p}_1|}\ln\left(\frac{t_1^+-m^2}{t_1^--m^2}\right),$$
$$I_2=\frac{2}{(t_1^+-m^2)(t_1^--m^2)}, \tag{2.16}$$
$$I_3=-\frac{1}{k\cdot r}I_1,$$

with $t_1^\pm=m^2-k\cdot r\pm 2|\vec{k}||\vec{p}_1|$ in terms of the $\vec{k}+\vec{r}=0$ frame quantities

$$|\vec{k}|=\frac{1}{\sqrt{s_1}}[(k\cdot r)^2-k^2r^2]^{1/2},$$
$$|\vec{p}_1|=(\tfrac{1}{4}s_1-m^2)^{1/2}.$$

The $T^{(2)}$ contractions are found quite simply from those for $T^{(1)}$ provided, as mentioned earlier, the p_3 integration does not differ (as it might for experimental reasons). Referring back to the substitutions described after Eq. (2.13), $T^{(2)}{}_{\lambda\nu}{}^{\lambda\nu}(-r,q)$ and $q^\sigma q^\lambda T^{(2)}{}_{\sigma\nu\lambda}{}^{\nu}(-r,q)$ are obtained from (2.14) and (2.15), respectively, by the replacements $k^2\to q^2$ and $s_1\to s_2$.

At this point, it behooves us to specify the r-integration procedure. By performing a trivial azimuthal integration, changing variables, and determining the integration region by the requirement that the c.m. angle between the vectors $\vec{P}_1\equiv\vec{k}+\vec{r}$ and $\vec{k}$ be real[18] we find[19]

$$\int_{\substack{\rm physical\\ \rm region}}d^4r=-\frac{\pi}{4}\frac{1}{[(k\cdot q)^2-k^2q^2]^{1/2}}\int dr^2ds_1ds_2\theta(D), \tag{2.17}$$

where

$$D\equiv\begin{vmatrix} r^2 & k\cdot r & r\cdot q\\ k\cdot r & k^2 & k\cdot q\\ r\cdot q & k\cdot q & q^2\end{vmatrix}. \tag{2.18}$$

Of course, $s'\geq 16m^2$, $s_1\geq 4m^2$, and $s_2\geq 4m^2$. Also, it should be evident by now that $k\cdot r$ and $r\cdot q$ are used interchangeably (as variables) with s_1 and s_2, respectively, in many of our expressions.

Although we found (2.17) adequate for our numerical work, it is useful to specify the exact integration limits. To this end, we introduce the variable $\phi>0$, $\phi_i>0$ via

$$\cosh\phi\equiv\frac{k\cdot q}{(k^2q^2)^{1/2}},$$
$$\cosh\phi_1\equiv\frac{k\cdot r}{(k^2r^2)^{1/2}}, \tag{2.19}$$
$$\cosh\phi_2\equiv-\frac{r\cdot q}{(r^2q^2)^{1/2}}.$$

Then

$$D = -r^2k^2q^2[\cosh\phi - \cosh(\phi_1+\phi_2)]\ [\cosh\phi - \cosh(\phi_1-\phi_2)]. \tag{2.20}$$

This leads to $\phi \geq \phi_1+\phi_2$ since $\cosh\phi \geq \cosh\phi_i$ by energy conservation. So[20]

$$\int_{\text{physical region}} d^4r = \frac{\pi}{\sinh\phi}\int r^2dr^2\theta(\phi-\phi_{10}-\phi_{20})\int_{\phi_{10}}^{\phi-\phi_{20}}\sinh\phi_1d\phi_1\int_{\phi_{20}}^{\phi-\phi_1}\sinh\phi_2d\phi_2, \tag{2.21}$$

with

$$\cosh\phi_{10} = \frac{4m^2-k^2-r^2}{2(k^2r^2)^{1/2}},$$
$$\cosh\phi_{20} = \frac{4m^2-r^2-q^2}{2(r^2q^2)^{1/2}}. \tag{2.22}$$

In the event k^2 and/or q^2 vanish, the ϕ_i are not well defined, so we revert back to the use of Eqs. (2.17) and (2.18). Suppose $k^2=0$ (the $q^2=0$ case follows trivially by symmetry):

$$\int_{\text{physical region}} d^4r = -\frac{\pi}{4k\cdot q}\int_{r_+^2}^{r_-^2}dr^2\int_{4m^2}^{s_1^{\max}}ds_1 \times\int_{4m^2}^{s_2^{\max}}ds_2. \tag{2.23}$$

From (2.18),

$$s_2^{\max} = -r^2\frac{k\cdot q}{k\cdot r} - q^2\frac{k\cdot r}{k\cdot q} + r^2 + q^2. \tag{2.24}$$

For a given physical value of r^2, s_1 is maximum when $s_2^{\max}=4m^2$. Choosing the appropriate root by energy conservation leads to

$$s_1^{\max} = r^2 + \frac{k\cdot q}{q^2}\{r^2+q^2-4m^2 + [(r^2+q^2-4m^2)^2 - 4q^2r^2]^{1/2}\}. \tag{2.25}$$

Finally, r^2 is restricted to those values for which $s_1^{\max}\geq 4m^2$. We have

$$r_\pm^2 = -k\cdot q + 4m^2 \pm k\cdot q\left(1-\frac{16m^2}{s'}\right)^{1/2}, \tag{2.26}$$

where $r_+^2 = r_-^2$ at $s'=16m^2$ as required. When $k^2=q^2=0$,

$$s_1^{\max} = -r^2\left(\frac{s'}{4m^2-r^2}-1\right). \tag{2.27}$$

We can now get values for $\tilde{\sigma}_i$ given in (2.7) by a Gaussian quadrature integration routine. That is, Eqs. (2.7) and (2.11)–(2.18) are collected together [the $t_i^{(2)}$ expressions follow by the aforesaid simple substitutions], and the last three integrals are done numerically with care taken in the placement of points for small $|r^2|$, s_1, and s_2. (Recall that the seven integrations indicated at the outset—neglecting a trivial azimuthal one—have been reduced to three by combining Lorentz invariance and factorization.) The explicit limits discussed above can be used to speed up the program and as checks. Figure 3 displays the results for several sets of k^2 and q^2 values.

It is seen in Fig. 3 that the asymptotic constant cross sections for a given k^2 and q^2 are reached when $s' \gtrsim 1000\max\{m^2, -k^2, -q^2\}$. This is consistent with the point at which $\ln^3 s'/s'$ can be neglected [see Eq. (2.1)]. It is gratifying to note that we recover the known 6.4-μb asymptotic limit (1.1) in the $k^2=q^2=0$ case; the energy dependence of this case is a new and useful result of our calculation. Notice that the general cross section scale in the asymptotic limits is characterized crudely by[21]

$$[(m^2-\tfrac{1}{4}k^2)(m^2-\tfrac{1}{4}q^2]^{-1/2},$$

a result of the fact that the photon masses change the minimum value of the electron propagator denominators over the region of s_1, s_2, and r^2 where the cross-section contribution is largest. This region is given by s_1, s_2 near (but not at) their threshold values $4m^2$, and for $|r^2|$ near its mini-

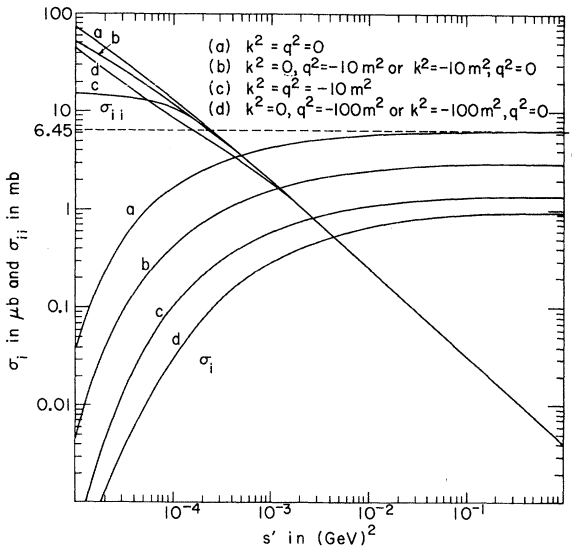

FIG. 3. The "generalized" cross sections (2.7) and (2.8) as a function of the square of the c.m. energy, s', for various (spacelike) photon mass values in units of μb and mb, respectively.

mum value. There the electron propagators conspire to peak at the same place with a decrease in the size of this peaking with an increase in $-k^2$, $-q^2$, and/or m^2.

It is interesting that as a result of gauge invariance the photon propagator does not further enhance the peak contribution. This is seen analytically by the dominant term in (2.11), which is $r^4(k\cdot q)^2$ in the curly brackets, the r^4 numerator canceling the r^{-4} from the propagators. Physically, we have the electromagnetic interaction of two systems, each with over-all zero charge, so the lowest multipole moment of the interaction currents must vanish.[22] For this reason, any approximation *must* be gauge-invariant.

The change in the thresholds for s_1 and s_2 from $4m^2$ to some higher value, say s_0, will also decrease the cross sections, but not as drastically as one might expect. For $k^2=q^2=0$, we have found numerically that the scale reads roughly $(m^2 s_0)^{-1/2}$ for $s_0 \lesssim 1000m^2$ rather than something like[23] s_0^{-1}. This is because phase space vanishes as $s_i \to 4m^2$ and the major cross-section contribution comes from $s_i \gtrsim 40m^2$.

As an interesting contrast we turn to the single-pair cross section (2.8). From Eqs. (2.6) and (2.14), we obtain

$$\tilde{\sigma}_{ii}(s',k^2,q^2)=\frac{2\pi\alpha^2}{s'}\left(\frac{s'-4m^2}{s'}\right)^{1/2}\{-2+(k^2+q^2-s'-2m^2)I_1'-(2m^2+k^2)(2m^2+q^2)I_2' +[(k^2+q^2)(s'-m^2)+m^2(s'-4m^2)]I_3'\}. \tag{2.28}$$

The quantities I_i' can be read from (2.16) after replacing r by q. For real photons, (2.28) reduces to

$$\tilde{\sigma}_{ii}(s',0,0)=\sigma_{ii}(s') =\frac{4\pi\alpha^2}{s'}\left\{\left(2+\frac{8m^2}{s'}-\frac{16m^4}{s'^2}\right)\ln\left[\left(\frac{s'}{4m^2}\right)^{1/2}+\left(\frac{s'}{4m^2}-1\right)^{1/2}\right]-\left(1+\frac{4m^2}{s'}\right)\left(1-\frac{4m^2}{s'}\right)^{1/2}\right\} \tag{2.29}$$

in agreement with the textbook expressions.[24] In the limit $s'\to\infty$, (2.29) yields (1.2).

We have included the single-pair cross-section curves in Fig. 3 for several k^2 and q^2 values. There are two points of interest which are evident in these plots. For small s' ($\sim 10m^2$), the scale of the cross section is roughly[25] $[m^2-\frac{1}{4}(k^2+q^2)]^{-1}$ and the peaking of the electron propagators is reduced as $-k^2$ and $-q^2$ increase. But in the regime $s'\gg 100m^2$, the minimum momentum transfer through the propagators has vanishing dependence on k^2 and q^2 as k^2/s', $q^2/s'\to 0$. Thus the scale of the logarithm in (1.2), m^2, which arises from the $\cos\theta_{p_1}=\pm 1$ integration region, is unchanged for large s'. Of course, the $1/s'$ over-all factor is also unchanged when s' is much larger than anything else. The curves show, as a result of all this, that there is weak dependence on k^2 and q^2 in the asymptotic region but strong scale changes near threshold.

It is important to note here that we have been interested in the k^2 and q^2 dependence of $A_{\beta\nu}{}^{\beta\nu}$ and $B_{\beta\nu}{}^{\beta\nu}$ rather than $\tilde{\sigma}_i$ and $\tilde{\sigma}_{ii}$. (The arbitrariness in these dependencies for the "generalized" cross sections should be obvious.) The former are the important subingredients in the reactions discussed later. Moreover, $\tilde{\sigma}_i$ and $\tilde{\sigma}_{ii}$ are not positive definite; for large $-k^2$ and $-q^2$ they decrease below zero, and other terms [for example, involving (2.15)] which vanish at $k^2=q^2=0$ must be kept in any approximations to the reactions of interest which contain these subgraphs in their dominant contributions. We will return to this aspect in the next section, but we merely remark here that the appropriate virtual-photon cross sections involving *all* contributions would be positive definite always.

While it has been easy to keep all terms in low-

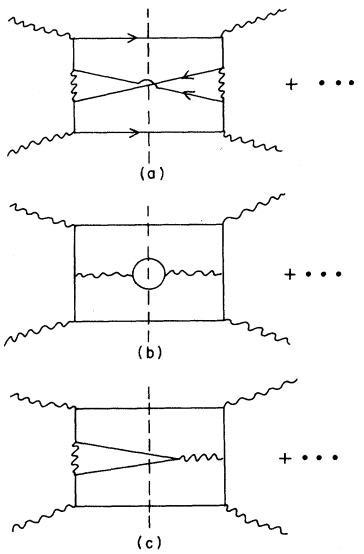

FIG. 4. The contributions to the cross section for $\gamma+\gamma\to e^+ + e^- + e^+ + e^-$ which vanish as $s'\to\infty$: (a) Interferences between even-C pair amplitudes; (b) squares of and interferences between odd-C pair amplitudes; (c) interferences between even-C and odd-C pairs.

est order of α for $\gamma+\gamma\to e^+ + e^-$, Fig. 4 illustrates the many cross-section terms neglected—for large s'—in the cross section for $\gamma+\gamma\to e^+ + e^- + e^+ + e^-$. It is seen that there are three classes of neglected cut graphs: (a) interference between two even-C pairs, (b) two odd-C pair squares and interference, and (c) interference between two even-C pairs and two odd-C pairs. The last is nonzero because the over-all charge-conjugation parity is even for both amplitudes. We have asked the reader to refer to the Appendix for arguments to the effect that all of these are down by a factor of s' (aside from powers of logarithms).

III. THE REACTIONS $\gamma+Z\to Z+e^+ + e^- + e^+ + e^-$ AND $\gamma\to Z\to Z+e^+ + e^-$

A. Dominant Contributions to the Cross Sections

According to the arguments in the Appendix (see also the discussion in Secs. IIIC and IIID), the dominant contribution for the cross section of Reaction (iii) corresponds to the absorptive part of the forward $\gamma+Z\to\gamma+Z$ amplitude depicted in Fig. 5(a). It is seen there that part of the graph is our dominant photon-photon kernel $A^{\rm dom}_{\beta\nu\alpha\mu}$ (the notation defined in Fig. 5 follows that of Sec. II). Here, of course, $k^2=0$ and we define $k^0\equiv\omega$ as the photon energy in the laboratory where the target with mass M is at rest.

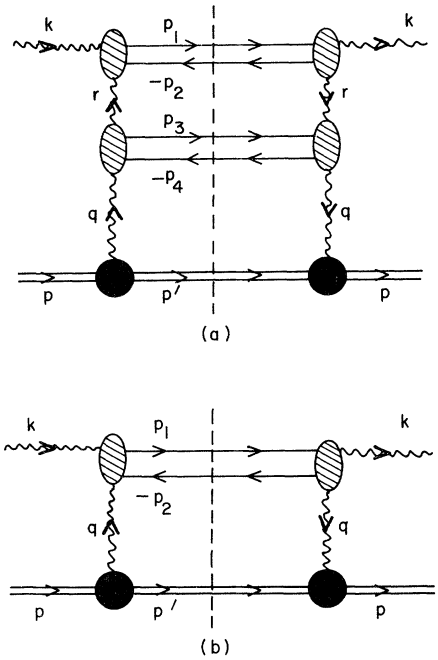

FIG. 5. The $\gamma+Z\to\gamma+Z$ forward absorptive parts which are related to the dominant cross section for (a) Reaction (iii) and (b) Reaction (iv) at high energy. The absorptive parts in Figs. 2(a) and 2(b) are attached in these two graphs to the absorptive part of the forward virtual Compton-Born amplitude for the target, so the shaded blobs are target form factors.

The multiperipheral character of the dominant term allows us to again factorize phase space and the absorptive amplitude by the identity

$$\delta^4\Big(\sum_i p_i + p' - k - p\Big) = \int d^4q\,\delta^4\Big(\sum_i p_i - k - q\Big) \times \delta^4(q+p'-p) \qquad (3.1)$$

as we did in Eqs. (2.2) and (2.3). An over-all azimuthal integration is simple, the q^0 integral is done easily due to the presence of an energy δ function, and $|\vec{q}|$ and $\cos\theta_q$ can be replaced in favor of the variables $s'\equiv(k+q)^2$ and q^2. Since we consider an unpolarized photon beam and target as well as the inclusion of all final spin states,

$$\sigma_{\rm iii} \cong \frac{Z^2\alpha}{16\pi}\frac{1}{(s-M^2)^2}\int_{q_-{}^2}^{q_+{}^2}\frac{dq^2}{q^4}\int_{s'_{\rm min}}^{s'_{\rm max}} ds' A^{\rm dom}_{\beta\nu}{}^{\beta}{}_{\mu}T^{\nu\mu}, \qquad (3.2)$$

where the square of the c.m. energy in Reaction (iii) has been denoted by $s=(k+p)^2=2M\omega+M^2$. The integration limits are given by[26]

$$q_\pm{}^2 = [-b\pm(b^2-4ac)^{1/2}]/2a, \qquad (3.3)$$
$$a = s/M^2,$$
$$b = 4\omega^2 - 2s'_{\rm min}(1+\omega/M),$$
$$c = s'_{\rm min}{}^2,$$

and by

$$s'_{\rm min} = 16m^2,$$
$$s'_{\rm max} = 2\omega|\vec{q}| + q^2(1+\omega/M), \qquad (3.4)$$
$$|\vec{q}| = (q^4/4M^2 - q^2)^{1/2}.$$

Here $q_-{}^2 < q_+{}^2 < 0$, and when $q^2\to q_\pm{}^2$, $s'_{\rm max}\to s'_{\rm min}$.

The target absorptive part in (3.2) reads

$$T^{\nu\mu} = F^2(q^2)(2p-q)^\nu(2p-q)^\mu \qquad (3.5)$$

for a spin-zero target with form factor F, or

$$T^{\nu\mu} = G_M{}^2(q^2)(q^2 g^{\nu\mu} - q^\nu q^\mu) + \frac{G_E{}^2(q^2)+\tau G_M{}^2(q^2)}{1+\tau}(2p-q)^\nu(2p-q)^\mu, \qquad \tau\equiv -q^2/4M^2 \qquad (3.6a)$$

for a spin-$\frac{1}{2}$ target with electric (magnetic) form factor G_E (G_M). However, as is seen in actual computation (and as is expected), our process here is very coherent, with less than 5% of the cross section coming from $-q^2\gtrsim 10^{-5}$ (GeV/c)^2. So, even for uranium, we can replace all electric charge form factors by unity with completely neg-

ligible error.[27] Also for protons and heavier nuclei, $M^2 \gg -q^2$ or $\tau \cong 0$, so that upon contraction with $A^{\text{dom}\ \beta}_{\beta\nu\ \ \mu}$ we could use $T^{\nu\mu} \cong (2p-q)^\nu (2p-q)^\mu$ to excellent approximation. The case where our target is an electron is of interest, however; hence the general approximation (omitting q^ν, q^μ terms by current conservation)

$$T^{\nu\mu} \cong q^2 g^{\nu\mu} + 4p^\nu p^\mu \tag{3.6b}$$

is extremely accurate for all of our cases of interest.

As in Eqs. (2.9) and (2.10), we can write

$$A^{\text{dom}\ \beta}_{\beta\nu\ \ \mu}(k,q) = (g_{\nu\mu}q^2 - q_\nu q_\mu)A(q^2,s') + [\,q^2 k_\nu k_\mu - k\cdot q(k_\nu q_\mu + q_\nu k_\mu) + (k\cdot q)^2 g_{\nu\mu}\,]B(q^2,s'), \tag{3.7}$$

so that the contraction in the integrand of (3.2) is

$$A^{\text{dom}\ \beta}_{\beta\nu\ \ \mu}T^{\nu\mu} \cong q^2(4M^2+2q^2)A(q^2,s') + [\,4q^2(k\cdot p)^2 - 4q^2 k\cdot p k\cdot q + 4M^2(k\cdot q)^2 + 2q^2(k\cdot q)^2\,]B(q^2,s'), \tag{3.8}$$

where $k\cdot p$ and $k\cdot q$ are used interchangeably with s and s', respectively, as independent variables. The point of all this is to use the fact that the invariant amplitudes

$$A(q^2,s') = -\frac{1}{(k\cdot q)^2}k^\nu k^\mu A^{\text{dom}\ \beta}_{\beta\nu\ \ \mu},$$

$$B(q^2,s') = \frac{1}{2(k\cdot q)^2}\left[A^{\text{dom}\ \beta\nu}_{\beta\nu} + \frac{3q^2}{(k\cdot q)^2}k^\nu k^\mu A^{\text{dom}\ \beta}_{\beta\nu\ \ \mu}\right] \tag{3.9}$$

can be evaluated in any convenient Lorentz frame.

We have already found $A^{\text{dom}\ \beta\nu}_{\beta\nu}$ in Sec. II [see Eq. (2.11), etc.], and, since we specialize to the $k^2=0$ case, the explicit integration limits given by (2.23)–(2.26) are useful here. The quantity $k^\nu k^\mu A^{\text{dom}\ \beta}_{\beta\nu\ \ \mu}$ is more painful to find, especially since the work needed in its calculation is inversely proportional to its contribution to (3.2); this projection always appears with q^2 coefficients in Eqs. (3.8) and (3.9), so it does not contribute to the leading cross-section contribution. Clarification of this point is made in the discussion below, but to check it we have actually calculated the projection.

We know from (2.3) and (2.9) that

$$k^\nu k^\mu A^{\text{dom}\ \beta}_{\beta\nu\ \ \mu} = \frac{1}{(2\pi)^8}\int \frac{d^4r}{r^4}\{[\,r^2 t_1^{(1)} + (k\cdot r)^2 t_2^{(1)}]k^\nu k^\mu T^{(2)}{}_{\lambda\ \ \nu\mu}^{\ \lambda}(-r,q) + r^2 t_2^{(1)} k^\sigma k^\lambda k^\nu k^\mu T^{(2)}{}_{\sigma\nu\lambda\mu}(-r,q)\}. \tag{3.10}$$

The first $T^{(2)}$ term in (3.10) can be found via

$$T^{(2)}{}_{\lambda\nu\ \ \mu}^{\ \lambda}(-r,q) = (g_{\nu\mu}q^2 - q_\nu q_\mu)t_1^{(3)}(r^2,q^2,s_2) + [\,q^2 r_\nu r_\mu - r\cdot q(r_\nu q_\mu + q_\nu r_\mu) + (r\cdot q)^2 g_{\nu\mu}\,]t_2^{(3)}(r^2,q^2,s_2). \tag{3.11}$$

These $t_i^{(3)}$ are calculated simply by substituting $k^2 \to r^2$, $r^2 \to q^2$, and $k\cdot r \to -r\cdot q$ ($s_1 \to s_2$) in our old $t_i^{(1)}$ expressions (2.12)–(2.16). On the other hand, the presence of the extra factors of k in the second $T^{(2)}$ term in (3.10) disallows such simple invariant-amplitude expansions. We consequently resort to a brute-force calculation facilitated somewhat by the fact that $k^2=0$. Using (2.4) and (2.5) with the appropriate replacements ($p_1 \to p_3$, $p_2 \to p_4$, $k \to -r$, $r \to q$), spin-summing leads to

$$k^\sigma k^\lambda k^\nu k^\mu T^{(2)}{}_{\sigma\nu\lambda\mu}(-r,q) = 8e^4\int \frac{d^3p_3}{E_3}\frac{d^3p_4}{E_4}\delta^4(p_3+p_4+r-q)(k\cdot p_4)(k\cdot p_3)\left[\frac{k\cdot(p_3+r)}{(p_3+r)^2-m^2} + \frac{k\cdot(p_3-q)}{(p_3-q)^2-m^2}\right]^2. \tag{3.12}$$

This invariant integral is straightforwardly done in the $-\vec{r}+\vec{q}=0$ frame with $-\vec{r}$ chosen as the z axis and $\vec{k}$ chosen to lie in the x-z plane. After the d^3p_4 and $d|\vec{p}_3|$ integrations are removed via the δ function, ϕ_{p_3} occurs only in the numerator and so the final θ_{p_3} integration is analytically simple but long. The cumbersome details do not seem to warrant a listing here.

The cross section for the companion Reaction (iv) is dominated by the absorptive part of the forward $\gamma + Z \to \gamma + Z$ amplitude shown in Fig. 5(b). (The relative unimportance of the Compton-type contribution is discussed later and in the Appendix.) Following the steps leading to Eq. (3.2), we have

$$\sigma_{\text{iv}} \cong \frac{Z^2\alpha}{16\pi}\frac{1}{(s-M^2)^2}\int_{q_-^2}^{q_+^2}\frac{dq^2}{q^4}\int_{s'_{\min}}^{s'_{\max}} ds' B_{\beta\nu\ \ \mu}^{\ \beta} T^{\nu\mu}, \tag{3.13}$$

with the carryover of (3.3) and (3.4), except that now $s'_{\min} = 4m^2$. It must be mentioned that this reaction already has been well studied—the famous

Bethe-Heitler pair production—but for comparison purposes we also treat it here. The ease with which its treatment goes through once the machinery for Reaction (iii) has been developed is motivation enough.

Again, the coherent nature of the photoproduction of small-mass particles allows the replacement of $B_{\beta\nu}{}^{\beta}{}_{\mu}T^{\nu\mu}$ [see Eqs. (2.6) and (2.9)] by the expression (3.8) if A and B are replaced by $t_1^{(1)}(k^2=0, q^2, s')$ and $t_2^{(1)}(k^2=0, q^2, s')$. The evaluation of these latter quantities follows by the appropriate substitutions in Eqs. (2.12)–(2.16).

It is useful in our numerical work to develop positivity conditions on the invariant amplitudes A and B. This is easily done by considering the virtual-photon cross section for $\gamma(k)+\gamma(q)\to$ four electrons, Reaction (i), where the first photon beam k is real and unpolarized and the second photon beam q is spacelike and has helicity λ_q. Averaging over the helicity of $\gamma(k)$ leads to the positive definite

$$\sigma_i(s', q^2; \lambda_q) = -\tfrac{1}{2} f \epsilon^{*\nu}_{\lambda_q}(q) A^{\mathrm{dom}}_{\beta\nu}{}^{\beta}{}_{\mu} \epsilon^{\mu}_{\lambda_q}(q), \quad (3.14)$$

in which f denotes the off-mass-shell normalization and relative velocity factors. In the $\vec{k}+\vec{q}=0$ c.m. frame, our choices for the transverse polarization vectors are ($\lambda_q=\pm1$; see Ref. 28)

$$\epsilon^{\mu}_{\pm}(q) = \mp\frac{1}{\sqrt{2}}(0, \hat{x} \pm i\hat{y}) \quad (3.15)$$

and the longitudinal polarization vector is ($\lambda_q=0$)

$$\epsilon^{\mu}_{0}(q) = \frac{1}{(-q^2)^{1/2}}(|\vec{q}|, -q_0\hat{z}), \quad (3.16)$$

with $\hat{k}=\hat{z}$. In this frame $|\vec{q}|=|\vec{k}|=\omega$.

It is simple to combine (3.14)–(3.16) with (3.7); we find that

$$\begin{aligned} \sigma_i(s', q^2, \pm1) &\equiv \sigma_{\mathrm{trans}} = \tfrac{1}{2} f[(k\cdot q)^2 B + q^2 A], \\ \sigma_i(s', q^2, 0) &\equiv \sigma_{\mathrm{long}} = \tfrac{1}{2} f[-q^2 A], \end{aligned} \quad (3.17)$$

so

$$(k\cdot q)^2 B \geq -q^2 A \geq 0. \quad (3.18)$$

Thus for $q^2<0$, $B\geq0$ and $A\geq0$.

We should relate these virtual-photon cross sections to the diagonal quantity $\tilde{\sigma}_i$ used in Sec. II. From (2.7)—noting that $1/2s'$ plays the role of f there—and (3.7),

$$\begin{aligned} \tilde{\sigma}_i(s', 0, q^2) &= \tfrac{1}{4} f[2(k\cdot q)^2 B + 3q^2 A] \\ &= \tfrac{1}{2}(2\sigma_{\mathrm{trans}} - \sigma_{\mathrm{long}}). \end{aligned} \quad (3.19)$$

One sees why for sufficiently negative q^2 we can have $\tilde{\sigma}_i<0$—as verified numerically. As $q^2\to0$, all roads lead to the correct total cross section $\tilde{\sigma}_i(s', 0, 0)=\sigma_{\mathrm{trans}}=\sigma_i(s')$. This discussion goes through for $\tilde{\sigma}_{ii}$ *mutatis mutandis*—$A(q^2, s')$ is replaced by $t_2^{(1)}(0, q^2, s')$, etc.

B. Numerical Results for the Dominant Contributions

A fivefold Gaussian numerical integration routine has been used to obtain values of σ_{iii} for different s and for different targets (nuclear or electron). Two integrals are specified in (3.2); since $k^2=0$, Eq. (2.23) is most convenient for the specification of the other three. We remind the reader that the initial ten integrations (disregarding a trivial over-all azimuthal one) have been reduced to these five by exploiting the factorized nature of our dominant cut graphs. Similarly, a twofold numerical integration has been performed in (3.13) for σ_{iv}—a reduction from four initial integrations.

The allocation of points in the computing programs is a delicate matter since the dominant regime is at very small $|q^2|$ and s' for Reaction (iv) and at very small $|r^2|$, s_1, and s_2 for Reaction (iii). The latter has somewhat larger average values for $|q^2|$ and s' than the former since the four-electron kernel peaks at large s'. The peaking in this small region of phase space can be stretched out and the computer time shortened considerably by changing to logarithmic variables. For example, we have used $x=\ln(s_1/4m^2)$, etc. Also, critical cancellations in $q_+{}^2$ of (3.3) and $r_+{}^2$ of (2.26) can be circumvented by unrationalizing the radicals into denominators. With all this in mind, a run for (iii) at a given s took only a minute or so on the CDC 6600, and a run for (iv) less than a second. There were not so many points needed, after all, since small q^2 squeezes the upper and lower limits together in the inner integrals.

To get a feeling for the q^2 range of importance, we have plotted histograms of percentages of cross section in logarithmic intervals in Fig. 6 for both

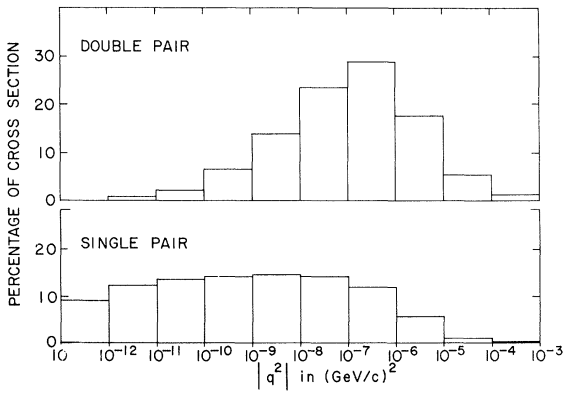

FIG. 6. The percentage of cross section for the dominant contributions to Reactions (iii) and (iv) in logarithmic $|q^2|$ intervals for proton targets at $\omega=10$ GeV. These results are essentially independent of the target (be it a nucleus or an electron).

Reactions (iii) and (iv) at $\omega = 10$ GeV and for proton targets. (Electron targets and, aside from the factor of Z^2, all nuclear targets give the same result.) The first bit of information evident here is the importance of extremely small $|q^2|$ values demonstrating the high degree of coherency. More interesting is the emphasis on relatively smaller values of $|q^2|$ in Reaction (iv). This is a result of the peaking at small s' for $\gamma+\gamma\to e^+e^-$ whereas the four-electron mode stays constant once its peak is reached as s' increases. Hence in (iii) there is a struggle between the decrease in the product of the $\gamma+\gamma\to e^+e^-+e^+e^-$ kernel and $1/q^4$ as $|q^2|$ grows and its increase ($s'\approx s'_{\max}$) as $s'_{\max} \sim 2\omega|q^2|$ grows. The leading logarithm comes from large s' in (iii), in contrast to (iv) where it comes from small s'. It really makes little difference whether we are talking about electrons or heavier targets since the energy transfer $|q_0| = -q^2/2M \ll M$ even for $M = m$ over most of the important q^2 regime.

The total cross sections as a function of energy are given in Fig. 7.[29] It is seen there that the cross section for Reaction (iv) quickly reaches the high-energy Bethe-Heitler formula (1.4) which includes the nonvanishing corrections to the leading logarithm. On the other hand, Reaction (iii) has a cross section always substantially below (1.3) which does not include the nonleading-logarithm corrections. These corrections are necessarily large and negative since the average s' value is not large enough for the asymptotic value of the four-electron kernel to be a good approximation; also, the fact that the relatively larger values of q^2 are important leads to some suppression through the scale change of the product of the kernel and $T^{\nu\mu}$, (3.8). The conclusion here is that a careful numerical evaluation of the leading contributions to (iii) is quite important even for an order-of-magnitude estimate. In order to make our results definite, we give numerical values at several energies for the cross section of Reaction (iii) in Table I.

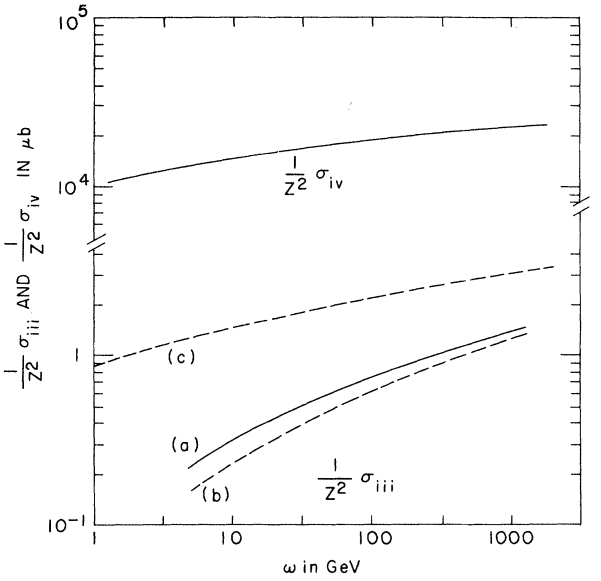

FIG. 7. The energy dependence of the dominant contributions to the cross sections for Reactions (iii) and (iv). The curves (a) and (b) refer to proton and electron targets, respectively. The asymptotic curve (c) is found from Eq. (1.3). For Reaction (iv), electron and proton targets give the same result which, in the energy range displayed, is indistinguishable from the asymptotic expression (1.4) which is more than a leading-logarithm approximation. According to Ref. 11, the electron curve for (iv) should be reduced by ~13%. This correction arising from the interference between exchange diagrams is not taken into account in our calculation.

C. Estimates of the Neglected Contributions

There are several contributions which have been neglected in our estimate of the rate for Reaction (iii). All of the *amplitudes* can be classified into three broad categories (see Fig. 8): single, double, and triple target electromagnetic couplings. Let us consider first the reasons for neglecting the double and triple couplings.

The coherent parts of the graphs in Figs. 8(b), 8(c), and 8(d), with Z dependences Z^2, Z^2, and Z^3, respectively, do not contribute to the cross section in the limit $M\to\infty$. The incoherent remainders in Figs. 8(c) and 8(d) do not contribute when $s\to\infty$, while the incoherent part of Fig. 8(b) contributes cross-section terms with the nucleon mass as scale (and the odd-C pair is very soft). For any energy regime, we conclude that the double and triple target couplings correspond to scales in the cross section much smaller than m^{-2} and can be neglected. This is true even for large Z and for interference terms between these amplitudes and the single-coupling amplitude.

The remaining cross-section terms which have been disregarded comprise part of the square of the single-coupling amplitude in Fig. 8(a). They correspond to the nonmultiperipheral cut graphs made up of the cut graphs in Fig. 4 tied onto a cut target line [e.g., see Figs. 1(b) and 1(c) in Ref. 8]; we will denote them as NMP cut graphs. These are more important here than the analogous graphs (Fig. 4) in Reaction (i) were, since we now integrate over s'. Indeed, as in single Bethe-Heitler pairs, the small-s' region gives rise to a very large cross section and the NMP cut graphs can have the m^{-2} scale too. According to the discussion in the Appendix, however, they are down from

TABLE I. Cross sections for Reactions (iii) and (iv) at photon energies of 10, 50, and 500 GeV. $\Delta\sigma_{iii}$ is the contribution of the $A(q^2, s')$ amplitude which must be added to σ_{iii} for the complete dominant cross section. The superscript s denotes the effect of screening for $Z=1$.

ω (GeV)	$Z^{-2}\sigma_{iii}$ (μb)	$Z^{-2}\Delta\sigma_{iii}$ (μb)	σ^s_{iii} (μb)	$\Delta\sigma^s_{iii}$ (μb)	$Z^{-2}\sigma_{iv}$ (mb)	σ^s_{iv} (mb)
10	0.28	0.04	0.27	0.04	14.4	9.3
50	0.53	0.06	0.50	0.06	17.3	9.3
500	1.10	0.07	0.91	0.07	21.5	9.3

the dominant part by a log factor.

An immediate guess then is that the NMP contribution should be about 10% of our calculation based on the cut graph in Fig. 5(a) [for $\omega \gtrsim 10$ GeV, $\ln(\omega/m) \gtrsim 10$]. We have not performed a careful evaluation of this portion (even a gauge-invariant subportion requires an inordinate amount of work; one needs more than just the leading logarithm for accuracy). On the other hand, there are decent reasons for believing that the first guess is close to the right answer. First, note the resemblance of this contribution to the single Bethe-Heitler rate: Both get their large contributions from small s' peaking, both have the m^{-2} scale, and both have the single $\ln(\omega/m)$ energy dependence. Thus we can obtain an estimate of the neglected NMP cut graphs by multiplying the cross section in Eq. (1.4) by $(\alpha/\pi)^2$. [Each new $e^2\int d^3p(2\pi)^{-3}$ in QED contributes α/π; indeed, the numerical factors in the expressions in Eqs. (1.1), (1.3), and (1.5) are essentially $(\alpha/\pi)^2$ times those in Eqs. (1.2), (1.4), and (1.6), respectively.] The ratio of this estimate to the dominant contribution runs about 25%–10% for $\omega = 10$–500 GeV.

Corroboration of the above estimate can be found in Table I. There one sees that the amplitude $A(q^2, s')$ (really, the ingredient $k^\nu k^\mu A^{\text{dom}\ \beta}_{\beta\nu\ \ \mu}$) adds

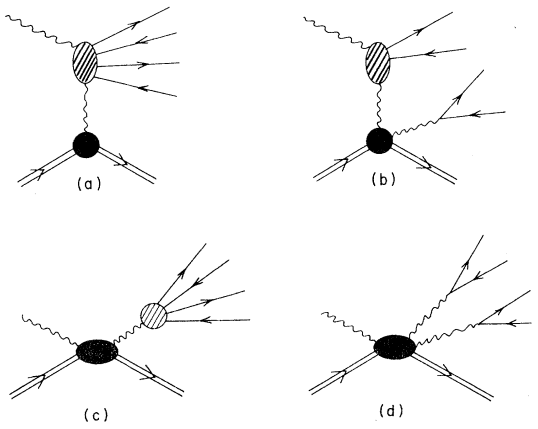

FIG. 8. The amplitudes for Reaction (iii). Categories (a), (b), (c), and (d) represent single, double, and triple target electromagnetic couplings, respectively.

very little to the numerical answer. Since this contribution is also down by a logarithm, its careful evaluation may be a mirror of the neglected terms. We are heartened by the fact that this adds less than 15% at $\omega = 10$ GeV, a percentage which decreases in energy as a log-dominated contribution would.

There are other encouraging signs regarding the NMP cut graphs (remember that these are the only contributions which have a chance of changing our result significantly). For instance, the Pauli principle which manifests itself through negative interference terms (all of which are in the NMP graphs) should be a factor. We expect to find important cancellations among the odd-C pair amplitudes whose contributions are peaked for small s' values where the identical electrons are closer together. On the other hand, there is little important overlap in phase space for our dominant piece—see Sec. III D—where the emphasis of larger s' corresponds to one hard and one soft pair. The interference terms (in the NMP graphs) between amplitudes whose squares make up the dominant cut graphs effect a smaller cancellation of these "squares." This is correlated with the fact that they are down by a logarithm. As an example, the odd-C pair muon trident amplitude in $\mu^\pm + Z \to Z + \mu^\pm + \mu^+ + \mu^-$ has important cancellations between exchange graphs. Cross-section measurements[30] on lead have verified this suppression by concentrating on that part of phase space where the identical muons have considerable overlap. A different experiment which could look at both very-high- and very-low-energy muons would get a large unsuppressed contribution from the even-C pair amplitude. Moreover, an interesting cancellation among NMP graphs has been seen in a recent calculation[31] pertaining to this experiment which is certainly of interest to us.

Another important suppression of the NMP cut graphs relative to the dominant contribution comes from screening. Since smaller values of q^2 and s' are important in the neglected graphs, the atomic electron shielding is more effective there. In this regard, see the discussion in Sec. III D where the analogy between the NMP and Bethe-Heitler pairs should be kept in mind. Screening is not im-

portant for the $A(q^2, s')$ contribution (see Table I) due to the fact that its leading logarithm comes from larger s' (hence larger q^2).[32]

After all that has been said here, we still cannot guarantee that the corrections from the other graphs will be small. The numerical coefficient could be large, although we could find no examples of this in the literature. (Recall that we are not talking about the next corrections in a given cut graph, which often have large numerical coefficients representing important phase-space, exchange, and scale reductions.) In addition, the nonleading-logarithm corrections in the dominant graphs have been shown to be substantially negative for lower energies; they will probably be less pronounced in the NMP graphs. As for the overall sign of the neglected contribution, we guess that it will probably be positive since many of the interference terms vanish by charge-conjugation symmetry [when tied to a cut nucleon line, Fig. 4(c) is a counterexample].

What happens if an electron is the target? Then everything is still pretty much the same although the amplitude in Fig. 8(b) then will also contribute to the $[\ln(\omega/m)]^{-1}$ correction. Notice that the small reduction in Eq. (1.4) for an electron[11] comes from exchange effects and corroborates our assertion that the exchange graphs in NMP contributions should not reduce significantly our result. Both get their dominant contribution from phase-space regions where the identical electrons have little overlap.

For targets with small Z, the atomic electrons will contribute significantly since the produced electrons are so light. One must combine the electron and the proton cross sections together for hydrogen targets.[33] Besides screening, the case for large Z brings up the question concerning higher-order $Z\alpha$ corrections. These multiphoton exchange effects corresponding to the Coulomb field that the final-state electrons see subtract away 10% or so from the Bethe-Heitler cross section for lead.[34] The corrections may be somewhat larger for our process in view of the presence of an additional low-energy pair.

D. Effects of Screening and Energy Threshold Cuts

Considering the numbers given in Table I, we hope that the photoreaction (iii) can be seen in the near future, in which case it becomes worthwhile to deal with experimental questions such as screening and energy threshold cuts. Since we have a bubble- or streamer-chamber experiment in mind, angular restrictions will be less important.

Screening of the nuclear charge due to atomic electrons is of course important at large distances, or, equivalently, small momentum transfers. From Fig. 6, however, we find that, although this serves to suppress the background coming from photoproduction of single pairs where smaller $|q^2|$ values are more important, it still leaves us a considerable rate for double pairs produced in the relatively larger $|q^2|$ region. To actually calculate the effect of screening, we multiply the target part $T^{\nu\mu}$ by the square of the atomic form factor[35]

$$F_a = \left(1 - \frac{1}{a^2 q^2}\right)^{-1}, \tag{3.20}$$

where $a \cong (111/m)Z^{-1/3}$ is the atomic radius. For $\omega = 10$ GeV and $Z = 1$, the rate for Reaction (iii) is reduced by about 4%, while Reaction (iv) suffers a reduction of 35%. We conclude that screening will not be a major factor in detecting double pairs.

More important is the effect of energy threshold cuts. It is well known that in multiperipheral processes the first pair (momenta p_1 and p_2) absorb most of the incoming energy. For a four-prong signal to be visible we must require that the second pair also carry at least ~100 MeV or so. We have calculated the cross section for Reaction (iii) by integrating over only that part of phase space where this condition is satisfied. We note that for fixed q^2, s', r^2, s_1 and s_2 (remember that integration over these variables is done numerically), the minimum value of $(p_{30} + p_{40})$ is obtained when the vector $\vec{r}$ lies in the plane of $\vec{k}$ and $\vec{q}$. The five integrations are now done subject to the condition that $(p_{30} + p_{40})_{\min}$ be greater than 100 MeV. In this case the reduction in σ_{iii} ranges from 39% to 25% for ω between 10 and 50 GeV, and stays almost constant at 25% for $\omega \geq 50$ GeV. In determining trigger requirements and background separation, experimentalists must take into account such important reductions which extend into the high-energy regime.

The experimental problem of separating the four-electron signal from multiple interaction events has already been discussed[8]; we have little to add at this stage. We will say that no problem arises from hadron production (e.g., from subsequent $\pi^0 \to 4e$) since the scale for the complete rate must be in terms of hadron masses. By far the biggest problem is pure QED: One cm divided by a radiation length in bubble chambers is of the same order of magnitude as α/π.

IV. THE REACTIONS $e^\pm + e^- \to e^\pm + e^- + e^+ + e^- + e^+ + e^-$ AND $e^\pm + e^- \to e^\pm + e^- + e^+ + e^-$

Our study of Reactions (v) and (vi) is oriented towards estimating the effect of kinematical cuts on their rates. The two-photon intermediate state

in the process

(vii) $e^{\pm}+e^{-}\to e^{\pm}+e^{-}+\Gamma$

has been studied in some detail[2,3] in order to extract information about photon-photon interactions, with particular attention paid to the case when Γ consists of hadronic states with even charge parity. Reactions (v) and (vi) would then be regarded as a background to such processes with their [see Eqs. (1.5) and (1.6)] considerably larger cross sections. As discussed in the Introduction, there are important nonleading negative corrections to (1.5) and (1.6). However, here we are interested in estimating much more important corrections—the drastic reductions (in the leading terms themselves) due to various experimental thresholds. For this purpose we shall use an equivalent-photon approximation which gives the leading term correctly.

When the momenta transferred to the colliding beams are small, the differential cross section for (vii) is effectively given by[36]

$$\frac{d\sigma}{dE_1'\,dE_2'\,dk^2\,dq^2}\cong\left(\frac{2\alpha}{\pi}\right)^2\frac{E^2+E_1'^2}{2E^2}\,\frac{E^2+E_2'^2}{2E^2}\,\frac{1}{k^2q^2}\,\frac{\sigma_{\gamma\gamma}(s',k^2,q^2)}{s'}\,, \tag{4.1}$$

where we have denoted the initial (final) energies of the leptons by E (E_1', E_2'). The quantity of interest, $\sigma_{\gamma\gamma}$, is of course the virtual-photon–photon cross section $\gamma\gamma\to\Gamma$. For Reactions (v) and (vi), $\sigma_{\gamma\gamma}$ is obtained from (2.7) and (2.8), respectively. In these cases Eq. (4.1) can be used to obtain only the leading contribution (as $E\to\infty$) to the total cross section, since it obviously neglects interference of diagrams with the final leptons interchanged, etc. In the usual equivalent-photon approach one sets $k^2=q^2=0$ in $\sigma_{\gamma\gamma}$. However, we have seen in Sec. II the important effect of the photon masses which regulate the scale of σ_i for $-k^2$, $-q^2\gtrsim m^2$. These last conditions were in fact assumed in the derivation of (4.1), and it is precisely on such effects that we focus our attention.

We shall compute $\sigma(E, s'_{\rm th}, \theta_{\rm min})$, which incorporates the effect of experimental cuts on the invariant mass $\sqrt{s'}$ of Γ and on the minimum angle for the detection of leptons. With a suitable change in the integration variables, we obtain

$$\sigma(E,s'_{\rm th},\theta_{\rm min})=\int_{s'_{\rm th}}^{4E^2}ds'\int_{s'/4E}^{E}d\omega_2\int_{k^2{}_{\rm min}}^{k^2{}_{\rm max}}dk^2\int_{q^2{}_{\rm min}}^{q^2{}_{\rm max}}dq^2\,\frac{1}{4\omega_2}\,\frac{d\sigma}{dE_1'\,dE_2'dk^2dq^2}\,, \tag{4.2}$$

where we have used $s'=4\omega_1\omega_2$, with $\omega_1=E-E_1'$ and $\omega_2=E-E_2'$ the energies of the virtual photons. $k^2{}_{\rm min}$ ($k^2{}_{\rm max}$) is given by

$$k^2=2(m^2-EE_1'+pp_1'\cos\theta_1)\,, \tag{4.3}$$

with $\theta_1=\theta_{\rm min}$ ($\theta_1=\pi-\theta_{\rm min}$). We shall consider the symmetric situation where $q^2{}_{\rm min}$ ($q^2{}_{\rm max}$) is obtained by using the same $\theta_{\rm min}$ ($\pi-\theta_{\rm min}$) for θ_2 in

$$q^2=2(m^2-EE_2'+pp_2'\cos\theta_2)\,. \tag{4.4}$$

To the four integrations indicated in (4.2) we must add three more needed to obtain σ_i when computing $\sigma_v(E, s'_{\rm th}, \theta_{\rm min})$. For our purpose in this section, however, it is sufficient to approximate the numerical results of Sec. II by a simple analytic expression:

$$\sigma_i(s',k^2,q^2)\approx\left(1-\frac{16m^2}{s'}\right)^{\gamma}\times\frac{m^2}{[(m^2-\frac{1}{4}k^2)(m^2-\frac{1}{4}q^2)]^{1/2}}\sigma_i(\infty)\,, \tag{4.5}$$

where $\sigma_i(\infty)\cong 6.45$ μb from Eq. (1.1). It is seen that with $\gamma\approx 6$ the above expression is a very good approximation to the curves displayed in Fig. 3. We have used this expression for $\sigma_{\gamma\gamma}(s', k^2, q^2)$ in (4.1), which when substituted into (4.2) yields $\sigma_v(E, s'_{\rm th}, \theta_{\rm min})$. The results are shown in Fig. 9. For $s'_{\rm th}\gg 16m^2$ and $\theta_{\rm min}\gg m/E$, we obtain

$$\sigma_v(E,s'_{\rm th},\theta_{\rm min})\cong 2\left(\frac{\alpha}{\pi}\right)^2\frac{m^2}{E^2}\left(\frac{1}{\sin\frac{1}{2}\theta_{\rm min}}-\frac{1}{\cos\frac{1}{2}\theta_{\rm min}}\right)^2\times\sigma_i(\infty)\ln^2\left(\frac{4E^2}{s'_{\rm th}}\right)\,, \tag{4.6}$$

which shows that the scale of σ_v is now given by $(E\sin\frac{1}{2}\theta)^{-2}$ rather than m^{-2} [remember that $\sigma_i(\infty)\sim 1/m^2$].

We have distinguished between angular and energy threshold cuts because we believe these to be experimentally more meaningful than a qualitative description of such reductions collectively as "threshold effects." For comparison and following the suggestion of Greco[12] we have also drawn on Fig. 9 the curve

$$\text{“}\sigma_v(E, s'_{th})\text{”} = \frac{1}{6}\left(\frac{\alpha}{\pi}\right)^2\left(\frac{16m^2}{s'_{th}}\right)\sigma_i(\infty) \times\left(\ln\frac{4E^2}{m^2}\ln\frac{64E^2}{s'_{th}}\right)^2, \quad (4.7)$$

which reduces to (1.5) for $s'_{th}=16m^2$ [for simplicity we have used the common variable s'_{th} as in Eq. (24) of Ref. 12]. Equation (4.7) is expected to describe experiments where no attempt is made to detect the electrons or positrons which serve as virtual-photon sources, while Eq. (4.6) is valid when these leptons are "tagged." This may be necessary in future colliding-beam experiments as discussed by Brodsky *et al.*[3] In this case the above calculations show that the background from Reaction (v) will be extremely small for $\theta_{min} > 1°$.

The same procedure is repeated to obtain $\sigma_{vi}(E, s'_{th}, \theta_{min})$. We substitute $\tilde{\sigma}_{ii}(s', k^2, q^2)$ as given in (2.28) for $\sigma_{\gamma\gamma}$ in Eq. (4.1), which is then used in (4.2), and a 4-dimensional numerical integration using Gaussian quadratures yields $\sigma_{vi}(E, s'_{th}, \theta_{min})$. This is plotted in Fig. 9 for $E=1$ GeV and different values of θ_{min} as a function of s'_{th}.

We can now discuss our results for σ_{vii} in terms of $\sigma_{\gamma\gamma}$, which, as we shall see, determines the essential features of the curves in Fig. 9.

(a) Dependence on θ_{min}. We see that

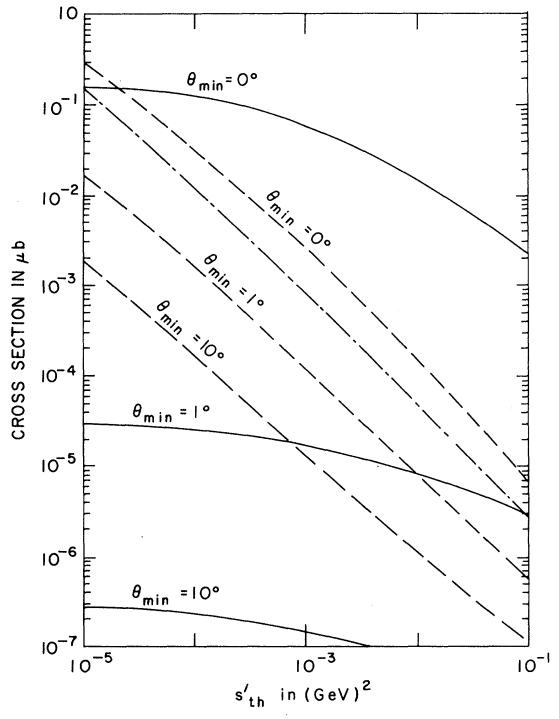

FIG. 9. σ_v (continuous lines) and $10^{-4}\sigma_{vi}$ (dashed lines) as a function of s'_{th} for different values of θ_{min}. The dot-dashed line is obtained from Eq. (4.7) and is to be compared with σ_v at $\theta_{min}=0°$. Beam energy is 1 GeV.

$\sigma_v(E, s'_{th}, \theta_{min})$ depends strongly on θ_{min}. This can be traced to the fact that the scale of $\tilde{\sigma}_i$ is roughly $(k^2q^2)^{-1/2}$ for $|k^2|$, $|q^2|$ much larger than m^2 (which is the case for $\theta_{min} \gg m/E$). On the other hand, $\sigma_{vi}(E, s'_{th}, \theta_{min})$ has a much milder dependence on θ_{min}. This is because the scale changes in $\tilde{\sigma}_{ii}$ occur mainly in the small-s' ($\approx 10m^2$) region, which we exclude, while for large enough s' the cross section depends weakly on k^2 and q^2 (see the discussion at the end of Sec. II).

(b) Dependence on s'_{th}. The roles are reversed here. Since $\tilde{\sigma}_{ii}$ peaks at small values of s' and vanishes like $\ln s'/s'$ for large s' (Fig. 3), a cut in this parameter appreciably reduces σ_{vi}, which now behaves roughly as $1/s'_{th}$. However, as $\tilde{\sigma}_i \sim$ constant for large s', such a cut does not take away any major portion of σ_v as long as $s'_{th} \ll 4E^2$.

We emphasize that our aim in this section has been to obtain the reductions which the leading terms suffer because of some experimental conditions. For the $\gamma\gamma \to e^+e^-e^+e^-$ process such cuts will make its observation extremely difficult. In any case, numbers accurate enough to be compared with any future experiments to detect (v) or (vi) should include the nonleading terms, as similar experimental conditions will no longer allow an equivalent-photon approximation when the cross sections depend crucially on the masses of the virtual photons.

V. ABSORPTION OF HIGH-ENERGY COSMIC γ RAYS

It has been recognized that, due to single-pair creation, cosmic γ rays of sufficiently large energy ω can undergo important absorption in the presence of the universal black-body radiation (possibly a remnant of a violent "big-bang" early stage).[15] When $\omega \gtrsim 10^{14}$ eV one must take into account Reaction (ii) where the target photon corresponds to a black-body photon with energy $\epsilon \approx 10^{-4}$–10^{-3} eV (~3 °K) and for $\omega = 10^{15}$–10^{17} eV the absorption depth (mean free path) is on the order of 10^{23} cm. Although the high-energy γ rays may reappear through subsequent inverse Compton scattering, the trajectories will have been diffused, at the very least.

Since the cross section for single-pair creation decreases with increasing ω, one may be led to the conclusion that photons with energies as high as the most energetic protons observed (10^{22}–10^{23} eV) may have a mean free path as large as the universe (the "Hubble radius" $R_H \sim 10^{28}$ cm). This seems to indicate that future considerations involving even higher energies would be unaffected by such absorption and we could "see" highly energetic photons irrespective of the point of origin. We wish to make the point here (backed up by the calcula-

tions which follow) that because of the large constant cross section for *two-pair* production, Reaction (i), we will never see extragalactic photons from the edge of the universe.[9] Just when the single-pair cross section is small enough to see out to 10^{26} cm, the double-pair cross section adds a constant (in energy) absorption probability per unit path length $\sim 10^{-26}$/cm. No further increase in the mean free path occurs.

To quantify and compare the effect of the single- and double-pair annihilation channels, we follow the calculation of Gould and Schréder,[15] who considered the absorption due to process (ii) of γ rays passing through a photon gas. One is interested in the absorption probability per unit length, $d\tau/dx$, given by[37]

$$\frac{d\tau}{dx} = \frac{1}{4\pi}\int\int \sigma(s)n(\epsilon)(1-\cos\theta)d\epsilon d\Omega\,, \tag{5.1}$$

where $\sigma(s)$ is the cross section for real photons with c.m. energy $\sqrt{s}$, and $n(\epsilon)$ is the energy spectrum of the target (number of photons per unit volume and energy). For an incident photon of energy ω,

$$s = 2\epsilon\omega(1-\cos\theta)\,, \tag{5.2}$$

where θ is the angle between the incident and target photons. Changing variables using (5.2) we obtain

$$\frac{d\tau}{dx} = \frac{1}{8\omega^2}\int_{s_0/4\omega}^{\infty}\frac{n(\epsilon)}{\epsilon^2}d\epsilon\int_{s_0}^{4\epsilon\omega} s\sigma(s)ds\,; \tag{5.3}$$

$s_0 = 16m^2$ and $4m^2$ for processes (i) and (ii), respectively. An integration by parts gives

$$\frac{d\tau}{dx} = \frac{1}{8\omega^2}\int_{s_0}^{\infty} V\left(\frac{s}{4\omega}\right)s\sigma(s)ds\,, \tag{5.4}$$

where

$$V(\epsilon) = \int_{\epsilon}^{\infty}\frac{n(\epsilon)}{\epsilon^2}d\epsilon\,. \tag{5.5}$$

We shall limit ourselves to the black-body radiation in the universe since this is the most important medium for the absorption of γ rays. In this case,

$$n(\epsilon) = \frac{1}{\pi^2}\frac{\epsilon^2}{e^{\epsilon/kT}-1}\,; \tag{5.6}$$

hence

$$V(\epsilon) = -\frac{kT}{\pi^2}\ln(1-e^{-\epsilon/kt})\,. \tag{5.7}$$

For absorption through single-pair creation, we substitute (2.29) for $\sigma(s)$ and (5.7) in (5.4). The result, for $T = 3\,^{\circ}$K, is shown in Fig. 10.

We use $\tilde{\sigma}_i(s, 0, 0)$ as given in (2.7) for $\sigma(s)$ in (5.4) to calculate the absorption due to double-pair creation. The result, after performing a 4-dimensional numerical integration [3-dimensional for $\tilde{\sigma}_i(s, 0, 0)$] is displayed in Fig. 10 for $T = 3\,^{\circ}$K. We have checked that the parametrization used in the previous section,

$$\tilde{\sigma}_i(s, 0, 0) \approx (1 - 16m^2/s)^6\sigma_i(\infty)\,, \tag{5.8}$$

gives essentially the same results.

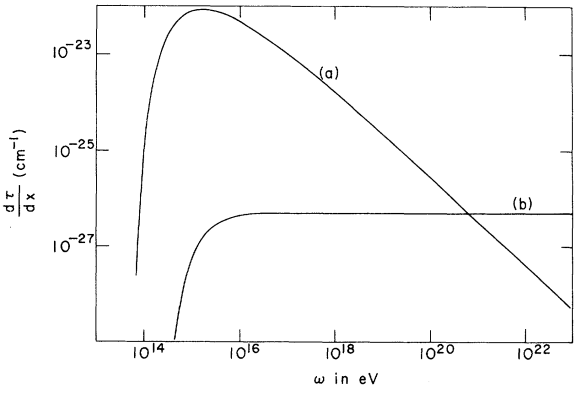

FIG. 10. Absorption probability per unit length as a function of γ-ray energy ω. The curves (a) and (b) correspond to absorption through single and double electron pair creation, respectively. The black-body temperature is 3 °K.

For fixed temperature T, one can obtain simple analytic results for $d\tau/dx$ in the two asymptotic limits $\omega \ll s_0/4kT$ and $\omega \gg s_0/4kT$. For this purpose (and also to compare with previous work) let us define the function $f(\nu)$ through

$$\frac{d\tau}{dx} = \frac{\alpha^2 m}{\pi}\left(\frac{kT}{m}\right)^3 f(\nu)\,, \tag{5.9}$$

where $\nu \equiv s_0/4\omega kT$. Hence

$$f(\nu) = -\frac{2}{\pi}\left(\frac{m\nu}{\alpha}\right)^2\int_1^{\infty}\xi\sigma(\xi s_0)\ln(1-e^{-\xi\nu})d\xi \tag{5.10}$$

for a black-body target. We can use the following asymptotic forms for the cross sections:

Single-pair creation.

$$\sigma_{ii}(\xi s_0) = \pi\left(\frac{\alpha}{m}\right)^2(\xi-1)^{1/2}[\,1+O(\xi-1)]\,, \qquad \xi - 1 \ll 1 \tag{5.11a}$$

$$\sigma_{ii}(\xi s_0) = \pi\left(\frac{\alpha}{m}\right)^2\frac{1}{\xi}[\,\ln(4\xi) - 1 + O(1/\xi)]\,, \qquad \xi \gg 1\,. \tag{5.11b}$$

Double-pair creation.

$$\sigma_i(\xi s_0) \cong (1-\xi)^6\sigma_i(\infty)\,, \quad \xi - 1 \ll 1 \tag{5.12a}$$

$$\sigma_i(\xi s_0) = \sigma_i(\infty)\,, \quad \xi \gg 1\,. \tag{5.12b}$$

With the above expansions we obtain

$$f(\nu)=(\pi\nu)^{1/2}e^{-\nu}[1+O(1/\nu)],\quad \nu\gg 1 \tag{5.13a}$$

$$f(\nu)=\tfrac{1}{3}\pi^2\nu\ln(0.47/\nu)[1+O(\nu\ln\nu)],\quad \nu\ll 1 \tag{5.13b}$$

for single-pair creation,[38] and

$$f(\nu)\cong\frac{2}{\pi}\left(\frac{m}{\alpha}\right)^2 6!\,\sigma_i(\infty)\frac{e^{-\nu}}{\nu^5}[1+O(1/\nu)],\quad \nu\gg 1 \tag{5.14a}$$

$$f(\nu)=\frac{2}{\pi}\left(\frac{m}{\alpha}\right)^2\zeta(3)\sigma_i(\infty)[1+O(\nu)],\quad \nu\ll 1 \tag{5.14b}$$

for double-pair creation, where ζ is the Riemann ζ function.

Our discussion at the beginning of this section was of course based on Eqs. (5.13b) and (5.14b). High-energy ($\geq 10^{21}$-eV) γ rays, while undergoing little absorption through single-pair production, are almost completely absorbed by double-pair creation when they pass through more than $\sim 10^{26}$ cm of black-body radiation. If such a radiation does extend throughout the universe, then we cannot expect to "see" any further than 10^{26} cm.

In passing, note that (5.14b) is valid for any annihilation process $\gamma+\gamma\rightarrow$ anything as long as the cross section stays constant in the high-energy limit. However, since other (e.g., hadronic) final states are produced at smaller rates, Reaction (i) remains the most important mechanism for absorption of very-high-energy γ rays. The total hadron asymptotic cross section has been estimated[39] to be about 0.3 μb—a factor of 20 smaller than the four-electron limit. In particular, the production cross section for a pair of point pions[3] is everywhere below that for a muon pair (discussed below). The conclusion we draw is that it would take unforeseen resonance structure in specific hadron channels to seriously increase the absorption already provided by (i). Also, remember that the effective c.m. energy $\sim 4\omega kT$ should be above threshold for any absorption process to be significant.

As far as other $\gamma\gamma$ reactions are concerned, they all appear to be negligible: (a) From Eq. (5.13b), $\gamma\gamma\rightarrow\mu\mu$ adds about 16% to $d\tau/dx$ at the critical energy 7×10^{20} eV where the two curves intersect in Fig. 10. The only change is in the mass, so that the peak here is $\sim(m_e/m_\mu)^2$ of the single-electron-pair peak and the two approach each other only when both are well below the double-electron-pair curve. (b) The asymptotic cross sections for $\gamma\gamma\rightarrow\mu\mu ee$ and $\gamma\gamma\rightarrow\mu\mu\mu\mu$ are $\sim 4\times 10^{-4}\sigma_i(\infty)$ (see Ref. 40) and $(m_e/m_\mu)^2\sigma_i(\infty)\sim 2\times 10^{-5}\sigma_i(\infty)$, respectively. Replacing the muon pairs by point pions leads to even smaller cross sections.[41] (c) $\gamma\gamma\rightarrow\gamma\gamma$ has a cross section which vanishes as $s\rightarrow\infty$ in lowest order (α^4); its s^{-1} scale is negligible compared with m^{-2}.[42] (For $s\sim m^2$, this is buried along with everything else under the single-pair peak.) (d) Adding more leptons and/or photons or going to higher order in, e.g., $\gamma\gamma\rightarrow\gamma\gamma$ can give rise to constant (or even logarithmic-powered) cross sections, but this is at the expense of too many powers of α/π relative to (i). (e) Weak interactions (e.g., $\gamma\gamma\rightarrow\nu\bar{\nu}$) have too many powers of α and G to be of interest at these energies.

We refer the reader to an earlier report[9] for discussions about absorption competition from a gas of radio-wave photon targets and the fate of the pairs after they are produced. That report also discusses the interesting cosmological point concerning the decrease of the ratio of the four-electron mean free path to the Hubble radius as we go back in time.

VI. CONCLUDING REMARKS

We have calculated the dominant contribution to the four-electron absorptive part of the forward virtual-photon–photon Feynman graph. This yields the mass and energy dependence of, for example, the cross section for $\gamma\gamma\rightarrow$ two lepton pairs at high energy. One can then see how the known asymptotic limits are approached with increasing energy. Beyond this, we have at our disposal a view of roles for $\gamma\gamma\rightarrow eeee$ analogous to those for $\gamma\gamma\rightarrow ee$ in various contexts. Although a direct measurement of the four-electron cross section is not in the immediate future, it enters indirectly into a number of interesting possibilities.

The photoproduction rate $\gamma Z\rightarrow Zeeee$ has been estimated in our work. We believe the theoretical uncertainties are under control and that the only real problem is an experimental one. Moreover, the energy dependence and screening differences between this rate and the multiple interaction background may be of help in background removal. This is, after all, a very high-order check of QED and may even serve as a probe of any anomalous four-electron contact term.[43]

The important change of scale in the four-electron kernel, remarked upon in earlier papers,[3,12,28] serves to suppress greatly the visible cross section for $ee\rightarrow eeeeee$ since the forward-angle and low-energy pairs escape unseen. We have seen that the form of the scale change is not easy to guess, and, even for an order-of-magnitude estimate, calculations as detailed as ours must be made.

The dominance of Reaction (i) over Reaction (ii)

at high energy leads to an interesting change in previous analyses concerning cosmic-photon absorption by residual photon gases in the universe. At higher and higher energies, the increasing mean free path for γ rays eventually levels off to a constant when (i) takes over [effectively, a scale change in $d\tau/dx$ due to (i)]. Such high-energy cosmic photons are a real possibility through, say, the by-products of cosmic-proton interactions (e.g., inverse Compton scattering off of the black-body gas). This may also have been of increasing importance in earlier stages of the universe where the temperature of the black-body gas may have been higher and the c.m. energies may have been greater.

ACKNOWLEDGMENT

We are grateful to Ed Yao and Byron Roe for their interest and participation in some of the calculations concerning the photoproduction experiment, and to Bob Gould for teaching us the state of the cosmic-photon-absorption art. One of us (R.W.B.) would like to acknowledge the hospitality of Brookhaven National Laboratory, where part of this work was carried out.

APPENDIX: HIGH-ENERGY BEHAVIOR OF RELEVANT GRAPHS

We present in this appendix some simple rules that enable one to read off the high-energy behavior $s^{\beta}(\ln s)^{\gamma}$ of the multiperipheral-type graphs that are calculated in detail here. We know from the work of Cheng and Wu[44] and Frolov, Gribov, and Lipatov[44] that the graphs in QED that give the leading logarithms and powers are the iteration of photon-photon scattering units, the multiperipheral graphs of Fig. 2(a).

The basic ingredient is to determine the order of the rightmost pole in the J plane after the graph is diagonalized across the two photon lines in the crossed channel. The order of the fixed pole, n, then determines the power of the logarithm $\gamma = n - 1$. This diagonalization has been done approximately with Mellin transforms and exactly with group-theoretical techniques for the multiperipheral model in strong interactions, and is well known in the literature. We will review the essential features in a heuristic way in this section.

Firstly, the position of the leading pole is at the highest nonsense value of the angular momentum for the state of maximum helicity flip in the crossed channel that is obtained by cutting across the two particles that are iterated. In particular for this case $J = |\lambda_1 - \lambda_2|_{\max} - 1$, where λ_1 and λ_2 are the helicities of the two internal photons in the t channel; it then follows that $|\lambda_1 - \lambda_2|_{\max} = 2$ and the position of the leading pole is at $J = 1$. This statement fixes the power of s, $\beta = 1$, in the corresponding high-energy behavior of the absorptive part:

$$A(s,t) \sim s(\ln s)^{\gamma} . \tag{A1}$$

To determine γ we need merely to compute the order of the fixed pole in the J plane, and this is obtained by the number of times the gauge-invariant kernel for photon-photon scattering is iterated in order $(e^4)^n$.

Since the photon must be exchanged at least once to give $\beta = 1$, $A(s,t) \sim s$, the simplest graph having this behavior is the graph corresponding to the absorptive part in Fig. 2. If the photon-photon scattering is iterated n times, the Mellin transform of the absorptive amplitude will have a structure of the form

$$a(J,t) = \frac{b_n(t)}{(J-1)^n} \tag{A2}$$

for all helicity components of the external photons and $b_n(t)$ is a residue function that can be calculated from the explicit graphs and is given in the work of Cheng and Wu.[44] We have simplified the discussion of the helicity amplitudes by considering the Mellin transform which give the absorptive part of the amplitude directly by the inverse transform

$$A(s,t) = \int dJ \, \frac{1}{(J-1)^n} b_n(t) s^J = s(\ln s)^{n-1} . \tag{A3}$$

Graphs of order $(e^4)^n$ with less than n iterations of the photon-photon kernel are down by logarithms and possibly even powers depending upon how many times the iteration takes place.

Examples of graphs that are down by a whole power with respect to those of Fig. 2(a) are those of Fig. 3, which are not multiperipheral and do not contain iterations of the photon-photon scattering kernel at all. Similarly, in higher orders the leading logarithms will come from graphs with the maximal number of iterations of the photon-photon scattering kernel as stated above.

In the process $\gamma + Z \to Z + e^+ + e^- + e^+ + e^-$, the non-multiperipheral graphs of Fig. 8(a) that are obtained by inserting the absorptive-part contribution of Fig. 4 into the square of the graph in Fig. 8(a) are only down by a logarithm from the calculated graphs of Fig. 5(a) and are perhaps the most dangerous of the neglected contributions. They are down by a logarithm because the graphs can be split apart by cutting two photons (photon-photon reducible once) only once as opposed to the multiperipheral graphs of Fig. 5(a) where two such pho-

ton-photon reductions can be made. The numerical sizes of such contributions are referred to in Sec. III. Other graphs that are not reducible in the same sense are the Compton graphs of Figs. 8(b), 8(c), and 8(d), and these are down by virtue of the large target mass M.

Of course graphs involving photon couplings to charged lines like those of Fig. 5 involve further logarithmic enhancements due to integration over small angular acceptances and give additional logarithms due to the presence of the photon propagator $D_F(q^2) = -i/q^2$. Contributions without the presence of the photon propagator will also be down by one power of the logarithm. The presence of such logarithms is well known in the literature[2] and will not be dealt with in detail here.

---

*Work performed, in part, under the auspices of the U. S. Atomic Energy Commission.

†Work supported, in part, by the National Science Foundation under Grant No. GP-33119.

[1]H. Cheng and T. T. Wu, Phys. Rev. Lett. 22, 666 (1969); Phys. Rev. 182, 1852 (1969); 182, 1868 (1969); 182, 1873 (1969); 182, 1899 (1969).

[2]N. Arteaga-Romero, A. Jaccarini, and P. Kessler, Compt. Rend. 269B, 153 (1969); 269B, 1129 (1969); V. E. Balakin, V. M. Budnev, and I. F. Ginzburg, Zh. Eksp. Teor. Fiz. Pis'ma Red. 11, 559 (1970) [JETP Lett. 11, 388 (1970)].

[3]S. J. Brodsky, T. Kinoshita, and H. Terazawa, Phys. Rev. Lett. 25, 972 (1970); Phys. Rev. D 4, 1532 (1971). For a general review, see S. J. Brodsky, in *Proceedings of the 1971 International Symposium on Electron and Photon Interactions at High Energies,* edited by N. B. Mistry (Laboratory of Nuclear Studies, Cornell Univ., Ithaca, N. Y., 1972).

[4]B. Bartoli *et al.*, Phys. Rev. D 6, 2374 (1972).

[5]H. Cheng and T. T. Wu, Phys. Rev. D 1, 3414 (1970); L. N. Lipatov and G. V. Frolov, Yad. Fiz. 13, 588 (1971) [Sov. J. Nucl. Phys. 13, 333 (1971)]. The reader should be made aware of the fact that some earlier papers give a wrong result for this limit.

[6]We dutifully follow the notation and conventions of J. D. Bjorken and S. D. Drell [*Relativistic Quantum Mechanics* (McGraw-Hill, New York, 1964); *Relativistic Quantum Fields* (McGraw-Hill, New York, 1965)]. Our units correspond to $\hbar = c = 1$ and $\alpha = e^2/4\pi$. Note that $\not{p} \equiv \gamma^\mu p_\mu$.

[7]This is the high-energy limit of Eq. (2.29). Note that the limits given in Eq. (2.2) of H. Cheng and T. T. Wu, Phys. Rev. D 2, 2103 (1970) and in Eq. (13-42) of J. M. Jauch and F. Rohrlich, *The Theory of Photons and Electrons* (Addison-Wesley, Reading, Mass., 1955) are missing a factor of 2 in front of the logarithm. This is not the factor of 2 discussed in the footnote found on p. 301 of the latter reference.

[8]Some of the photoproduction results have been reported earlier by R. W. Brown, I. J. Muzinich, B. P. Roe, and Y.-P. Yao [Phys. Rev. Lett. 28, 123 (1972)].

[9]Our cosmic-photon results are described by R. W. Brown, K. O. Mikaelian, and R. J. Gould [Astrophys. Lett. 14, 203 (1973)].

[10]V. G. Serbo, Zh. Eksp. Teor. Fiz. Pis'ma Red. 12, 50 (1970) [JETP Lett. 12, 39 (1970)]; Lipatov and Frolov, Ref. 5.

[11]Jauch and Rohrlich, Ref. 7, p. 378; A. I. Akhiezer and V. B. Berestetskii, *Quantum Electrodynamics* (Interscience, New York, 1965), p. 447. In Eqs. (1.3) and (1.4), we have neglected screening, $O(Z\alpha)$ corrections, and pair production off of the electrons surrounding the nucleus Z. For an electron target, $Z^2 = 1$ and 218 is replaced by 318 in Eq. (1.4) according to Eq. (11-67) of Jauch and Rohrlich (Ref. 7). Unfortunately, Eq. (32.29) of Akhiezer and Berestetskii would have 291.6 rather than 318.

[12]M. Greco [Nuovo Cimento 4A, 689 (1971)] obtains a larger numerical factor in his leading-logarithm estimate of Reaction (v) using Cheng-Wu techniques. However, we believe the method of calculation in this reference needs some modification since, for example, Greco's result for Reaction (vi) differs from well-known results. The identity of the electrons in the final states here should not change the leading logarithm.

[13]L. D. Landau and E. M. Lifshitz, Physik Z. Sowjetunion 6, 244 (1934). A careful assessment of this old reference would have taught us long ago to beware of simple power-counting in α.

[14]V. N. Baier and V. S. Fadin, Phys. Lett. 35B, 135 (1971).

[15]R. J. Gould and G. P. Schrêder, Phys. Rev. Lett. 16, 252 (1966); J. V. Jelley, *ibid.* 16, 479 (1966).

[16]There are actually 64 "cut diagrams" in a cross-section calculation, and their fourfold degeneracy is canceled by the $(2\,!2\,!)^{-1}$ statistical factor.

[17]W. N. Cottingham, Ann. Phys. (N.Y.) 25, 424 (1963).

[18]We are now talking about the over-all c.m. frame where $\vec{k} = -\vec{q}$ and $\vec{P}_2 \equiv -\vec{r} + \vec{q} = -\vec{P}_1 = -\vec{k} - \vec{r}$.

[19]T. W. B. Kibble, Phys. Rev. 117, 1159 (1960).

[20]This transformation has been used before in a different context by S. Nussinov and J. Rosner [J. Math. Phys. 7, 1670 (1966)].

[21]Our characterization is not an analytically derived result but rather a guess in rough agreement with the numerical results. We omitted the factors of $\frac{1}{4}$ in our earlier guess (Ref. 8).

[22]This is the same crucial role current conservation plays in, for example, $\nu_\mu + Z \to \mu^- + W^+ + Z$. See R. W. Brown and J. Smith, Phys. Rev. D 3, 207 (1971).

[23]One often finds in the literature remarks to the effect that thresholds furnish the scale for constant or logarithmically increasing cross sections. This counterexample serves as a caveat. See Sec. IV.

[24]Jauch and Rohrlich, Ref. 7, Eq. (13-40); Akhiezer and Berestetskii, Ref. 11, Eq. (32.27).

[25]Again, a guess mocking up the numerical results.

[26]The calculation of these limits is essentially the same as that described by Brown and Smith, Ref. 22.

[27]See the form-factor curves in Brown and Smith, Ref. 22. Because the process is so coherent, we neglect the incoherent nucleon scattering for large Z. Also,

incoherent scattering suffers an appreciable reduction from exclusion-principle effects on the nucleons.

[28]This basis is used in other related calculations described by I. J. Muzinich, L.-L. Wang, and J.-M. Wang [Phys. Rev. D 2, 1985 (1970)] and R. W. Brown and I. J. Muzinich [*ibid.* 4, 1496 (1971)]. The latter reference contains corrections of some of the misprints in the former reference.

[29]The proton and electron curves are about 10% higher on the average than those given in Ref. 8 due to the added contribution of the $A(q^2, s')$ amplitude.

[30]J. J. Russell *et al.*, Phys. Rev. Lett. 26, 46 (1971).

[31]M. N. Kobrinskii and F. F. Tikhonin, Yad. Fiz. 15, 1238 (1972) [Sov. J. Nucl. Phys. 15; 685 (1972)].

[32]The leading term in Bethe-Heitler pairs (and in the NMP cut graphs) is a Weizsäcker-Williams infrared logarithm from small q^2. This is the origin of only one of the two powers of logarithm in the dominant contribution. As $\omega \to \infty$, screening cuts off Bethe-Heitler pairs but the dominant rate continues to increase logarithmically.

[33]In general, we need to consider both the nuclear target (as shielded by the atomic electrons) and the electron targets including their screening by the nuclear charge. See Ref. 35.

[34]Akhiezer and Berestetskii, Ref. 11, pp. 445–446.

[35]K. J. Kim and Y.-S. Tsai, Phys. Lett. 40B, 665 (1972); SLAC Report Nos. SLAC-PUB-1105 and SLAC-PUB-1106, 1972 (unpublished). The atomic electron targets are also screened more effectively for Bethe-Heitler pairs than for our two-pair production. (See Ref. 33.) For $\omega = 10$ GeV, $Z = 1$, and $a \to a' = 7.87aZ^{-1/3}$ in Eq. (3.20), we have $\sim 15\%$ ($\sim 1\%$) reduction for a single (double) pair produced off of an electron target.

[36]R. J. Gould, Am. J. Phys. 39, 911 (1971). Equation (5.1) can also be derived using a calculation patterned after the noncollinear-beam discussion on p. 113 of J. D. Bjorken and S. D. Drell, *Relativistic Quantum Mechanics* (McGraw-Hill, New York, 1964).

[38]These agree with the formulas of Gould and Schrêder [Ref. 15; Phys. Rev. 155, 1404 (1967); 155, 1408 (1967)] when note is taken of the misprints and algebraic errors enumerated in Ref. 9. See some related formulas in G. R. Blumenthal and R. J. Gould, Rev. Mod. Phys. 42, 237 (1970).

[39]See Balakin *et al.* (Ref. 2), Brodsky *et al.* (Ref. 3), and Brown and Muzinich (Ref. 28). The c.m. energies are not high enough to take into account the newly seen rise in the pp cross section in the estimates which relate $\gamma\gamma \to$ hadrons to $\gamma p \to$ hadrons and $pp \to$ hadrons. Other estimates and their role in the absorption of extragalactic γ rays can be found in K. A. Ispiryan and S. G. Matinyan, Zh. Eksp. Teor. Fiz. Pis'ma Red. 7, 232 (1968) [JETP Lett. 7, 178 (1968)]; K. Terasaki-Okada, Prog. Theor. Phys. 49, 349 (1973).

[40]We have calculated this cross section by merely redoing the integrations described in Sec. II after changing the masses of one pair. The result is consistent with the analytic limit given by M. Masujima [Nucl. Phys. B24, 182 (1970)].

[41]Cheng and Wu, Ref. 7.

[42]Ispiryan and Matinyan, Ref. 39, give the forward differential cross section limit as $\sim 10^{-8}(\ln^4 s)/s$ μb/sr, with s in GeV^2. See also A. I. Achieser (Akhiezer), Physik Z. Sowjetunion 11, 263 (1937).

[43]R. Weinstein (private communication).

[44]H. Cheng and T. T. Wu, Phys. Rev. D 1, 2775 (1970); G. V. Frolov, V. N. Gribov, and L. N. Lipatov, Phys. Lett. 31B, 34 (1970).